Retinal input integration in excitatory and inhibitory neurons in the mouse superior colliculus *in vivo*

Carolin Gehr[1-4], Jérémie Sibille[1-4], Jens Kremkow[1-4]

[1]Neuroscience Research Center, Charité-Universitätsmedizin Berlin, Charitéplatz 1,10117 Berlin

[2]Bernstein Center for Computational Neuroscience Berlin, Philippstraße 13, 10115 Berlin

[3]Institute for Theoretical Biology, Humboldt-Universität zu Berlin, Philippstraße 13, 10115 Berlin

[4]Einstein Center for Neurosciences Berlin, Charitéplatz 1,10117 Berlin

Send correspondence to:
Jens Kremkow
Neuroscience Research Center
Charité - Universitätsmedizin Berlin
Charitéplatz 1
10117 Berlin, Germany
Phone: +49 30 450 639081
Email: jens.kremkow@charite.de
Web: kremkowlab.com, twitter.com/Kremkow

ABSTRACT

The superior colliculus (SC) is a midbrain structure that contains one of the highest densities of inhibitory neurons in the brain and, together with the thalamocortical visual system, it plays a key role in visually guided behaviors. The SC receives direct inputs from retinal ganglion cells (RGCs) but whether excitatory and inhibitory SC neurons differentially integrate retinal activity *in vivo* is still largely unknown. We recently established an extracellular recording approach using high-density electrodes to measure the activity of RGCs simultaneously with their postsynaptic SC targets *in vivo*, that allows addressing how SC neurons integrate RGC activity. Here, we employ this method to study the functional properties and dynamics that govern retinocollicular signaling in a cell-type specific manner by identifying GABAergic SC neurons using optotagging in anesthetized VGAT-ChR2 mice. We measured 305 monosynaptically connected RGC-SC pairs, out of which approximately one third of retinal afferents connect onto inhibitory SC neurons. We show that both excitatory and inhibitory SC neurons receive comparable strong RGC inputs, with functionally similar RGC-SC pairs showing stronger connections. Our results demonstrate that similar wiring rules apply for RGCs innervation of both excitatory and inhibitory SC neurons, which is unlike the cell-type specific connectivity in the thalamocortical system. Contrasting the similar RGC-SC connection strength, we observed that RGC activity contributed more to the activity of postsynaptic excitatory SC neurons than to the activity of postsynaptic inhibitory SC neurons. This implies that the excitatory SC neurons are more specifically coupled to RGC afferent inputs, while inhibitory SC neurons may integrate additional inputs from other sources. Taken together, our study deepens the understanding of cell-type specific retinocollicular functional connectivity and emphasizes that the two major brain areas for visual processing, the visual cortex and the superior colliculus, differently integrate sensory afferent inputs.

INTRODUCTION

The mouse superior colliculus (SC) is a midbrain structure that receives direct inputs from retinal ganglion cells (RGCs) (Ellis et al., 2016; Kremkow and Alonso, 2018). Together with the visual cortex (Glickfeld et al., 2013; Lashley, 1931; Niell and Scanziani, 2021; Petruno et al., 2013), the SC plays a key role in visually guided behaviors (Evans et al., 2018; Hoy et al., 2019; Shang et al., 2019, 2015; Wei et al., 2015). Intriguingly, the visual SC layers contain one of the highest densities of inhibitory (GABAergic) neurons in the brain (Kaneda et al., 2008; Ranney Mize, 1992) suggesting that inhibition plays a key role in visual processing within the SC. Indeed, inhibitory SC neurons (INs) are known to be involved in several sensory functions including surround suppression (Kasai and Isa, 2016) and motion processing (Barchini et al., 2018; Gale and Murphy, 2016), but also in the regulation of wakefulness (Zhang et al., 2019). However, how GABAergic SC neurons are recruited by their retinal inputs *in vivo* remains largely unknown (Shi et al., 2017). An understanding how RGC inputs are integrated by SC INs and SC excitatory neurons (EXNs) is crucial for reaching a mechanistic understanding of the computations within the SC microcircuit.

In sensory systems, the divergence of long-range afferent axons onto GABAergic and non-GABAergic neurons ensures a balance between excitation and inhibition (E/I) (Miller, 2016). For example, in sensory cortices, thalamic afferents differentially activate excitatory and local inhibitory neurons (Cruikshank et al., 2007; Ji et al., 2016) with a stronger drive onto inhibitory neurons compared to excitatory neurons (Bruno and Simons, 2002; Cruikshank et al., 2007; Gabernet et al., 2005; Gibson et al., 1999; Inoue and Imoto, 2006; Swadlow, 2003). This stronger drive on inhibitory neurons establishes an effective feedforward inhibition (Agmon and Connors, 1992; Bereshpolova et al., 2020; Gabernet et al., 2005; Kremkow et al., 2010a, 2010b; Sun et al., 2006) that balances the excitation from thalamic afferents (Isaacson and Scanziani, 2011) and contributes to sharpening stimulus feature selectivity (Lee et al., 2012). Moreover, this wiring motif can partly be linked to the response properties of cortical inhibitory neurons as they typically show higher firing rates, broader tuning, low selectivity and high sensitivity (Alonso and Swadlow, 2005; Bruno and Simons, 2002; Gibson et al., 1999; Kremkow et al., 2016; Porter et al., 2001; Swadlow et al., 2002) to facilitate feedforward inhibition in response to thalamic input. Despite the importance of this afferent wiring motif for sensory processing in the thalamocortical visual circuit, it is currently unknown whether the retinocollicular pathway follows similar or different principles.

We recently demonstrated that SC neurons can receive strong input from RGC axons *in vivo* (Sibille et al., 2022a). Moreover, around one third of retinocollicular synapses connect onto inhibitory neurons that form intrinsic connections within the SC (Whyland et al., 2020). These findings support the notion that an effective feedforward inhibition might also be at play in the retinocollicular system. But whether afferent inputs are differentially integrated by excitatory and inhibitory SC neurons,

similar to the thalamocortical system, is unknown. However, our previous study in the retinocollicular system lacks the cell-type specificity, and it remains an open question whether the strong drive is specific to inhibitory SC neurons or is a general property of retinocollicular connections, and thus cell-type independent. Therefore, whether there are any differences in connection strengths between RGCs that project to excitatory and inhibitory SC neurons is different remains elusive. In this study, we investigate how excitatory and inhibitory neurons in the SC integrate retinal inputs *in vivo*.

We aim to answer these questions by characterizing the properties of the long-range synaptic connections between RGC-SC pairs employing a set of measurements: 1. The connection efficacy is used to study how strongly excitatory and inhibitory SC neurons are driven by their RGC input. 2. The functional similarity is analyzed between connected RGC-SC pairs to examine whether comparable wiring motifs govern retinocollicular signaling in excitatory and inhibitory neurons. 3. Short-term dynamics of retinal activity are studied to estimate whether the retinal spiking pattern shows paired-spike enhancement on retinocollicular synapses. Finally, 4. the connection contribution is employed to investigate how tightly the SC activity is coupled to retinal spiking.

This study intends to generate a more detailed picture of cell-type specific retinocollicular innervation and to fill a gap concerning the different long-range functional connectivity motifs that exist along the visual pathways.

RESULTS

Recording excitatory and inhibitory neurons simultaneously with RGC axons in the mouse SC *in vivo*

To investigate the integration of retinal input in excitatory and inhibitory neurons in the SC *in vivo*, we recorded extracellular neural activity in the visual layers of SC in VGAT-ChR2 mice using high-density Neuropixels probes (Jun et al., 2017). We employed a tangential insertion approach to maximize the extent of visually driven channels in the SC (Fig. 1A) (Sibille et al., 2022a). Notably, we recently demonstrated that this approach allows us to not only measure spiking activity from SC neurons, but also to record electrical signals from retinal ganglion cell axons (RGC) that terminate at the SC (Sibille et al., 2022a). The somatic action potentials of SC neurons can be distinguished from the axonal action potentials of RGCs based on their spatiotemporal waveforms profile (Sibille et al., 2022a). RGC axonal waveforms are triphasic with a larger spatial spread (Fig. 1D left) while somatic SC neurons show a characteristic biphasic waveform profile (Fig. 1D, middle and right).

To study cell-type specific differences, we combined the Neuropixels recordings with an optogenetic identification strategy (optotagging) to identify GABAergic SC neurons in VGAT-ChR2-EYFP (Zhao et al., 2011) mice (Fig. 1A, B; data from n = 11 experiments and n = 9 mice included in the analysis, if not stated otherwise). In these transgenic mice, GABAergic neurons specifically express Channelrhodopsin-2 and can be identified upon blue light stimulation. To photo-activate a large proportion of GABAergic SC neurons using short light pulses (100ms pulses, 2Hz, 2.7 mW) we inserted the optic fiber perpendicularly to the Neuropixels probe (Fig. 1A, right, see Material and Methods). Using this recording and light stimulation configuration we could activate GABAergic SC neurons across an average of ~1.5 mm of SC tissue (light-activated range = 1.50 $\pm$ 0.41 mm, Fig. 1B) which also allowed us to record SC neurons along continuous retinotopy (Fig. 1C, right) in a cell-type specific manner (Fig. 1G). We used the visually evoked activity and continuous retinotopy to demarcate the boundaries of the SC (Fig. 1C). Moreover, for the characterization of excitatory and inhibitory classes of SC neurons, we limited our analysis to single units that were localized within the range of optogenetic stimulation (Fig. 1B/C, see Material and Methods). Cell types were characterized using a custom-written graphic-user-interface (GUI, see Material and Methods) to label units that were activated by the LED pulse as inhibitory neurons (INs, Fig. 1E, middle). These neurons were distinguished based on their reliable, short-latency responses to optogenetic stimulation during spontaneous (black screen) and visually evoked conditions (checkerboard stimulus, see Material and Methods). SC neurons that were not modulated by the LED pulses, but located within the light-activated range, were labeled as excitatory (EXNs, Fig. 1E bottom). As expected, retinal axons were not activated by the LED pulse (Fig. 1E, top), except for a few cases (4/326 RGCs) which were excluded from the connectivity analysis in this study. In total, we recorded

326 RGC axons and 680 SC neurons. Among the recorded SC neurons one third (31.2%) were GABAergic (Fig. 1G, n = 468 EXNs, n = 212 INs).

Having sorted the SC neurons into the cell classes using optogenetic stimulation (EXNs and optogenetically identified INs) we compared different spike waveform features to test whether SC neurons show differences in their waveforms. Characterizing the spike waveforms is commonly used in the cortex or hippocampus to differentiate between glutamatergic and GABAergic neurons (Lee et al., 2016; Moore and Wehr, 2013; Niell and Stryker, 2008). However, the separation based on differences in waveform features was not an adequate measure to separate SC EXNs from SC INs (Supplementary Fig. 1). This result is in line with findings by Essig et al. who did not observe a cell type specific difference between waveform features in the SC (Essig et al., 2021). Similar findings have been shown in the inferior colliculus (Ono et al., 2017), a neighboring midbrain structure, suggesting that waveform classification analyses used in the cortex are not suitable for distinguishing neurons in the midbrain.

To further characterize the response properties of the different cell classes (RGC, SC INs, SC EXNs), we measured their firing rates (FR) in response to a natural movie stimulus provided in Froudarakis et al. (2014) (Froudarakis et al., 2014) (see Material and Methods). We found that RGCs showed the highest FR (mean firing rate RGC = 11.3 $\pm$ 10.5 spikes/s, n = 326 EXNs; Fig. 1G, bottom). On average, the mean FR in SC INs (mean firing rate IN = 5.9 $\pm$ 6.0 spikes/s, n = 212 INs) was 1.8 times higher compared to that of SC EXNs (mean firing rate EXN = 3.2 $\pm$ 4.9 spikes/s, n = 468 INs, SC EXN vs SC IN $p = 3.1567\times10^{-15}$, SC EXN vs RGC $p = 4.8362\times10^{-40}$, SC IN vs RGC p = 2.738810^{-8}, two-sided Wilcoxon rank-sum test). Our results are in line with previous studies by Reid (1998, 2003) showing that RGCs show high mean firing rates (Kara and Reid, 2003; Usrey et al., 1998). Moreover, from other midbrain areas it is also known that GABAergic neurons show higher FRs compared to glutamatergic cells (Ono et al., 2017).

In summary, by combining Neuropixels recordings to measure the activity of RGC axons and SC neurons with optogenetic identification of GABAergic SC neurons, it becomes possible to measure monosynaptic retinocollicular connectivity *in vivo* and retinal innervation strength in a cell-type specific manner.

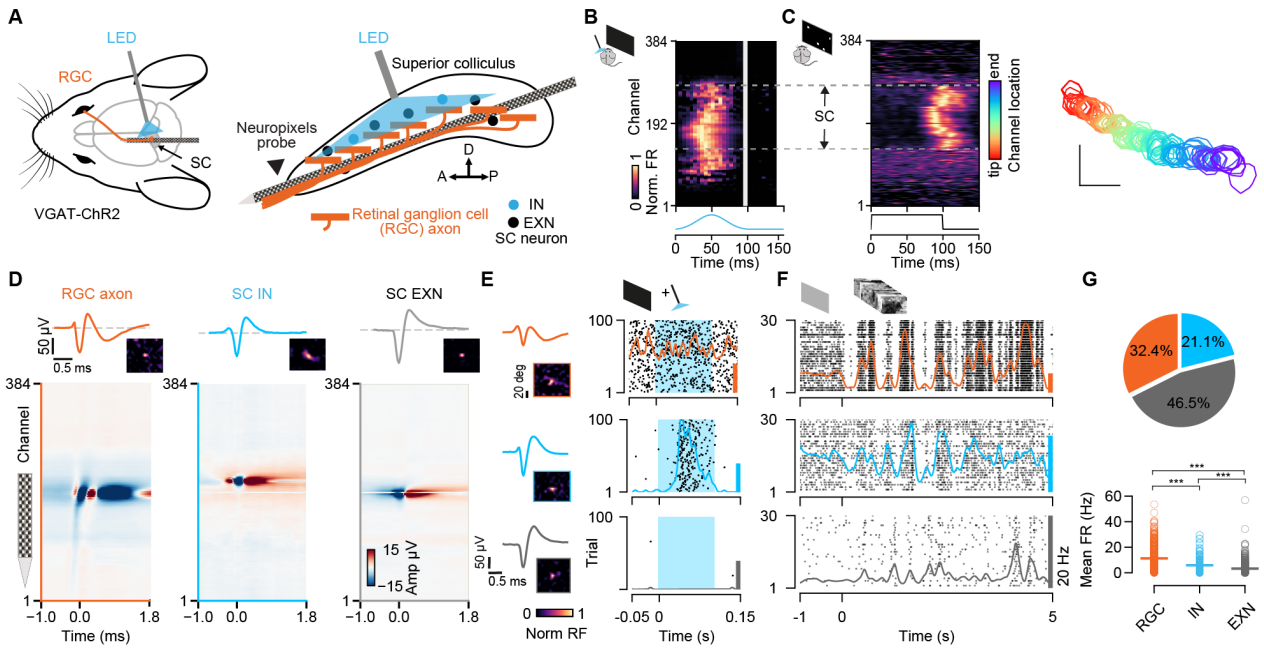

Fig. 1 Simultaneous extracellular recordings of RGC axons and SC neurons combined with optotagging identifies GABAergic neurons in VGAT-ChR2 mice. A, Recording configuration for tangential electrode insertion and optotagging in the visual layers of mouse SC. The optogenetic fiber is inserted perpendicularly to the Neuropixels probe to activate GABAergic cells in VGAT-ChR2 mice. RGC afferents (orange) project onto GABAergic (blue) and non-GABAergic (black) neurons in SC. **B,** Multi-unit response (MUA) to optogenetic stimulation along the 384 recording sites during the presentation of a black screen. The large spatial extend of the optogenetic activation is evident. Gray vertical bar = light artifacts induced by the LED stimulation. **C,** Visually evoked MUA during the presentation of a sparse noise stimulus along the recording sites. Receptive field contours of recording sites with high signal-to-noise ratio. The color code reflects the location within the SC. Scale bar represents 10 degree. **D,** Spatiotemporal waveform profiles. Single channel waveforms identified at the peak channel (top) and multi-channel waveforms (bottom) for RGC axon (left, orange) and inhibitory (middle, blue) and excitatory (right, gray) SC neurons. Receptive fields (RFs) indicate visually responsive neurons. **E,** Identification of SC cell-types via optotagging. Raster plots and peri-stimulus time histograms (PSTHs) for single-neuron responses to blue light pulses (100ms) presented under baseline conditions. Excitatory SC neurons (EXNs, bottom) and RGCs (top) do not respond to the LED pulse, while GABAergic SC neurons respond to the light pulse with an increase in spiking response (middle). Optogenetic stimulation period is highlighted in blue. The colored scale bars on the right represent 20 Hz firing rate. **F,** PSTHs and raster plots for different cell types shown in E in response to a natural movie stimulus (10s, 30 trials). Note the high firing rate in RGCs. **G,** Top: Proportion of identified GABAergic (INs, blue), non-GABAergic (EXNs, gray) SC neurons and retinal axons (RGCs, orange) populations. Note that around one third of the captured SC neurons are GABAergic (n = 326 RGCs, n = 468 EXNs, n = 212 INs). Bottom: Mean firing rates in response to a natural movie stimulus presented for 10s, 30 trials. Two-sided Wilcoxon rank-sum test.

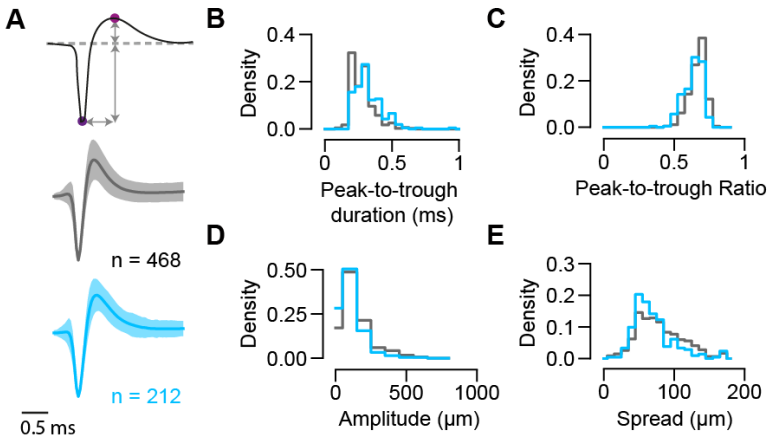

Supplementary Fig. 1 Spike waveform features analysis for GABAergic and non-GABAergic neuron populations in the SC. A, Top: Illustration of features extracted from single-channel waveforms (magenta circles indicate the trough and peak). Middle and bottom: Single-channel mean waveforms for non-GABAergic (gray; n = 468) and GABAergic (blue, n = 212, n = 9 mice) SC populations (mean±SEM). **B-D,** Distribution of waveform features extracted from single-channel waveforms for inhibitory and excitatory SC populations. Peak-to-trough duration represents the time between trough and peak ($p = 4.05\times10^{-10}$). Peak-to-trough ratio represents the ratio between amplitudes of peak and trough ($p = 4.45\times10^{-9}$). Amplitude is the absolute difference between trough and peak ($p = 1.38\times10^{-9}$). **E,** Distribution of waveform spread along the probe extracted from multichannel waveforms for GABAergic and non-GABAergic SC populations ($p = 1.58\times10^{-4}$, n = 468 EXNs, n= 212 INs, Two-sided Wilcoxon rank-sum test).

229 **Retinal input integration in excitatory and inhibitory SC neurons**

230 To study the monosynaptic retinocollicular connectivity *in vivo* and retinal innervation strength, we
231 identified putative monosynaptically connected RGC-SC pairs employing established cross-
232 correlation analysis (CCG) methods (Alonso et al., 2001; Bereshpolova et al., 2020; Sibille et al.,
233 2022a). A significant transient and a short-latency peak in the spike train CCG is a hallmark of
234 monosynaptic connectivity (Fig. 2A) and identifies connected RGC-SC pairs. We measured up to 98
235 monosynaptic connections in individual recordings, depending on the number of measured RGC
236 axons (Fig. 2C). In total, we identified 305 connected RGC-SC pairs, of which 29.8% were retinal
237 axons that connected onto GABAergic SC neurons (n = 214 connected RGC-SC EXN pairs, n = 91
238 connected RGC-SC IN pairs, Fig. 2B/D). This high yield in monosynaptically connected pairs was
239 due to the close proximity of the simultaneously recorded RGC axons and SC neurons on the high-
240 density electrode (Fig. 2D, bottom) (Sibille et al., 2022a). For most of the connected RGC-SC pairs
241 the peak channels on the electrode were on average 50-60 µm apart on the probe and hence within
242 SC (distance RGC-EXN: median = 40.0 µm, first quartile = 25.61 µm, third quartile = 62.1 µm;
243 distance RGC-IN: median = 51.22 µm, first quartile = 32.0 µm, third quartile = 83.08 µm). We found
244 a significant difference in peak channel distance between RGC-SC EXN and RGC- SC IN pairs with
245 longer distances between RGC axons and inhibitory SC neurons (p = 0.03287, two-sided Wilcoxon
246 rank-sum test), however, the effect size was small (Cohen's d = 0.0915). The maximum distance for
247 retinal axons and inhibitory SC neurons was 240 µm, while the peak channels of one RGC-SC EXN
248 pair were 960 µm apart. The latter pair might include a SC wide field neuron as these cells are
249 excitatory and their dendritic arbor widths have been reported to spread up to 900 µm (Gale and
250 Murphy, 2014).
251
252 To assess the connection strength between RGCs and excitatory and inhibitory SC neurons, we
253 calculated the connection efficacy (Usrey et al., 1999). The efficacy measures the connection
254 strength as the probability of an RGC spike triggering an action potential in the postsynaptic SC
255 neuron (see Material and Methods). We found highly diverse connectivity patterns for RGC-SC EXC
256 and RGC-SC IN pairs. RGC activity evoked robust firing in both SC cell types (Fig. 2E, top), however,
257 pairs with weak connection strength were also observed as recently described in Sibille et al. (2022a)
258 (Fig. 2E, bottom). Across the population, both SC cell types received similarly strong input from the
259 retina (efficacy RGC-SC IN: median = 4.54 %, Q1 = 2.2 %, Q3 = 7.96 %, maximum = 62.05 %, n =
260 91 connected pairs, Fig. 2F) compared to RGC-SC EXNs (efficacy RGC-SC EXN: median = 3.5 %,
261 Q1= 1.96 %, Q3 = 5.89 %, maximum = 41.12, n = 214 connected pairs). While we observed a
262 tendency for slightly stronger RGC-SC IN connections, this difference was not statistically significant
263 (p = 0.0534, two-sided Wilcoxon rank-sum test). In addition, we examined whether excitatory and
264 inhibitory cells show differences in their peak latencies in response to presynaptic retinal spiking.
265 However, we did not find a significant difference in peak latencies between RGC-SC EXN and RGC-

SC IN pairs (Fig. 2G, peak latency for RGC-SC EXN = 1.4 ± 0.3 ms, n = 214 connected pairs; peak latency for RGC-SC IN = 1.4 ± 0.4 ms, n = 91 connected pairs, p = 0.321, two-sided Wilcoxon rank-sum test).

Here, we set out to explore how RGC spikes drive the activity in postsynaptic excitatory and inhibitory SC neurons. We did not find a cell-type specific difference in connection strength and therefore conclude that inhibitory and excitatory SC neurons are innervated comparably strong and are both reliably driven by their retinal inputs.

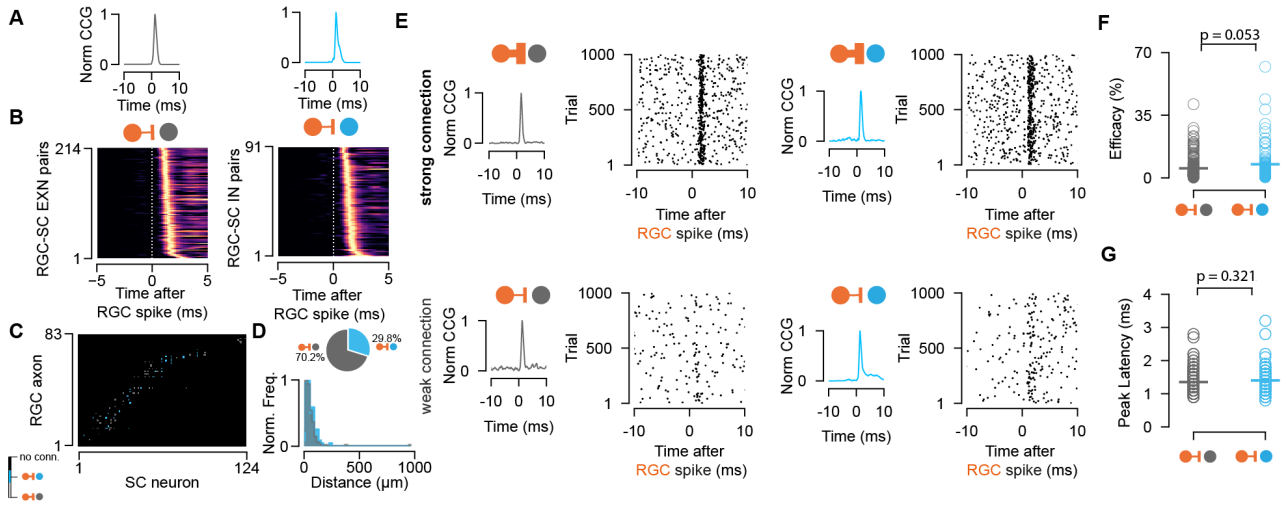

Fig. 2 Retinal innervation is similarly strong to excitatory and inhibitory SC neurons. A, Monosynaptically connected RGC-SC EXN (gray) and RGC-SC IN (blue) pairs are identified via cross-correlation analysis (CCG). **B,** CCGs of connected RGC-SC EXN and RGC-SC IN pairs sorted by their peak latency (n = 214 RGC-SC EXN, n = 91 RGC-SC IN, n= 11 recordings). **C,** Connectivity matrix from a single recording. Gray marks indicate connections onto excitatory SC neurons, blue marks indication connections onto inhibitory SC neurons. RGC axons and SC neurons are sorted by their peak channel along the electrode. **D,** Distribution of peak channel distances between RGC axons and connected SC neurons (p = 0.0328, two-sided Wilcoxon rank-sum test). Inset shows pie chart of identified RGC-SC IN and RGC-SC EXN pairs. **E,** Elicited SC spiking in response to firing of a presynaptically connected retinal ganglion cell (RGC). Raster plot shows SC firing to 1000 randomly selected RGC spikes. Both SC cell types show robust activation upon RGC spiking (top) but also weaker connections can be found (bottom). **F,** Synaptic efficacy as a measure for connection strength for RGC-SC EXN and RGC-SC IN connected pairs (p = 0.053, n = 214 RGC-SC EXN, n = 91 RGC-SC IN). **G,** Peak latency responses for RGC-SC EXN and RGC-SC IN pairs triggered on retinal spiking (p = 0.321). Two-sided Wilcoxon rank-sum test.

292 **Functional similarity of retinocollicular connections**

293 In sensory cortices, inhibitory neurons are less selective and receive a diverse and nonspecific set
294 of thalamic inputs compared to excitatory neurons that receive more specific thalamic inputs (Alonso
295 and Swadlow, 2005; Bruno and Simons, 2002). However, the selectivity and functional similarity
296 between RGCs and their excitatory and inhibitory target populations in SC remains largely unknown
297 (Shi et al., 2017). Despite both SC populations showing a similar innervation strength from retinal
298 axons, inhibitory neurons could sample from a more functionally diverse population of RGCs. To test
299 this, we characterized the functional similarity between the RGCs and their connected postsynaptic
300 SC neurons. To this end, we calculated the correlation coefficients between the trial-averaged
301 visually evoked activity of connected RGC-SC pairs in response to light and dark sparse noise stimuli
302 (r_{SL} & r_{SD}) as well as the natural movie stimulus (r_{NM}) (Fig. 3A/B, RGC-SC with high signal-to-noise
303 in their receptive, see Material and Methods). To quantify the overall functional similarity by a single
304 similarity value, we averaged the three correlation measurements (similarity = (r_{SL}+ r_{SD} + r_{NM})/3). A
305 similarity value of 1 corresponds to perfectly correlated visually driven responses, while a value of 0
306 signifies uncorrelated responses. In our data, the RGC-SC pairs span a wide range of functional
307 similarity, however, we found no significant difference between RGC-SC EXN and RGC-SC IN pairs
308 (similarity for RGC-SC EXN = 0.45 ± 0.15 and RGC-SC IN = 0.40 ± 0.17, n = 85 RGC-SC EXN pairs,
309 n = 29 RGC-SC IN pairs, p = 0.245, two-sided Wilcoxon rank-sum test, Fig. 3C). In a next step, we
310 correlated the connection efficacy measure to the similarity index. The synaptic efficacy was
311 positively correlated with the functional similarity of the connected pairs, with a stronger correlation
312 for RGC-SC IN pairs (RGC-SC EXN r = 0.29, p = 0.007; RGC-SC IN r = 0.471, p = 0.01, Fig. 3D).
313 Overall, we observed that functionally similar pairs are more strongly connected. However, we also
314 observed cases of relatively strong connected RGC-SC pairs (~10%) with low similarity (Fig. 3D),
315 suggesting that some SC neurons receive convergent input from a functionally more diverse pool of
316 RGC afferents (Sibille et al., 2022a). Our findings delineate that both RGC-SC EXN and RGC-SC
317 IN connected pairs are organized, while functionally similar properties between the pre- and
318 postsynaptic neuron are reflected in a stronger connection.
319

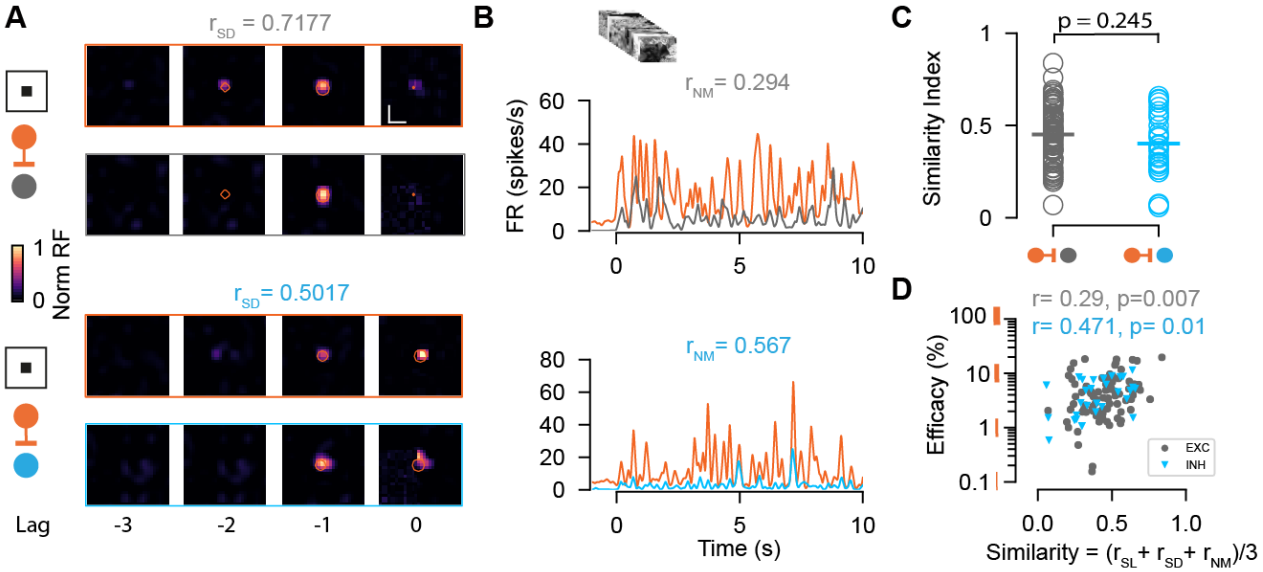

Fig. 3 Characterization of functional similarity between retinocollicular connected pairs. A, Spatiotemporal receptive fields (STRF) evoked by a dark sparse noise stimulus for RGC-SC EXN and RGC-SC IN connected pairs. The functional similarity of the RGC axon and the postsynaptic SC neuron is characterized by the correlation coefficient r_{SD}. **B,** Visually evoked activity in response to a natural movie stimulus for the connected pairs shown in A together with their correlation coefficient values r_{NM}. **C,** The overall functional similarity between the presynaptic RGC and the postsynaptic SC neurons is reflected in the similarity index calculated from the averaged correlation coefficients $(r_{SD} + r_{SL} + r_{NM})/3$ ($p = 0.245$, two-sided Wilcoxon rank-sum test, n = 85 RGC-SC EXN pairs, n = 29 RGC-SC IN pairs). **D,** Relationship between similarity index and connection efficacy (RGC-SC EXN $r = 0.29$, $p = 0.007$; RGC-SC IN $r = 0.471$, $p = 0.01$; Pearson correlation coefficient test; n = 85 RGC-SC EXN pairs, n = 29 RGC-SC IN pairs).

Paired-spike interactions of the retinocollicular connections

We showed that retinal spikes are efficient in driving SC activity for both excitatory and inhibitory neurons. As the timing of presynaptic activity has been assessed as a parameter that modulates postsynaptic firing (Zucker, 1989) and connection strength (Kara and Reid, 2003; Usrey et al., 1998), we wanted to know whether the temporal pattern of retinal activity has different effects on the synaptic efficacy of excitatory and inhibitory SC neurons. To that end, we studied the short-term dynamics (facilitation or depression) of the measured connections and performed a paired-spike analysis approach as described by Usrey and colleagues in 1998 (Usrey et al., 1998). A pair of retinal spikes (1st, 2nd RGC) was defined by its temporal firing patterns: inter-spike interval (ISI) and dead time. We selected RGC spikes for which a 1st RGC followed the 2nd RGC by a specific ISI (minimum ISI = 5ms, maximum ISI = 30ms). The dead time ensured that the 1st RGC was preceded by a minimum period without activity (30ms) (Fig. 4A).

We found that overall 2nd retinal spikes were more efficient in driving SC activity, and thus facilitating. This was true for both RGC-SC EXN (efficacy 1st RGC: median = 1.8 %, Q1 = 0.77 %, Q3 = 4.47 %; efficacy 2nd RGC: median = 2.66 %, Q1 = 1.16 %, Q3 = 6.07 %, p 1st vs 2nd = 3.13×10^{-25}, n = 214 pairs) and RGC-SC IN connected pairs (efficacy 1st RGC: median = 3.66 %, Q1 = 1.6, Q3 = 8.61; efficacy 2nd RGC: median = 4.33, Q1 = 2.03, Q3 = 8.25, p 1st vs 2nd = 1.68×10^{-6}, n = 91 pairs, Wilcoxon signed-rank test) (Fig. 4B, C). This effect is known as paired-spike enhancement and has been reported earlier in retinogeniculate (Mastronarde, 1987; Usrey et al., 1998) and geniculocortical (Usrey et al., 2000) connections. The majority of retinocollicular connected pairs showed paired-spike enhancement where 2nd retinal spikes were more effective in driving SC response (86.45% (185/214) RGC-SC EXN pairs, 80.22 % (73/91) RGC-SC IN pairs). The effect was more pronounced in RGC-SC EXN pairs where the 2nd retinal spike was 1.7 times as effective in driving responses in the postsynaptic SC neuron while for RGC-SC IN pairs, the 2nd retinal spike was only 1.3 times more efficacious in driving SC spiking. To quantify this observation, we calculated the paired-spike ratio (PSR = efficacy 2nd/efficacy 1st) which confirmed a higher facilitation effect for RGCs connecting into excitatory neurons (PSR RGC-SC EXN = 1.711 ± 1.14; RGC-SC IN: 1.281 ± 0.414, p = 0.00002582, Wilcoxon rank-sum, n = 305 pairs, Fig. 4D).

Previous work in the thalamocortical system has shown that weaker synaptic connections can be more strongly modulated compared to strong synaptic connections (Ferrarese et al., 2018). To test the notion that also in the retinocollicular system, connected pairs with lower efficacy in response to 1st RGCs show greater enhancement in response to the 2nd RGCs, we correlated the efficacy of the 1st RGC to the PSR (Fig. 4E). We found a negative correlation of efficacy to 1st RGC and PSR for both RGC-SC EXN (r = 0.3314, p = 7.0148×10^{-7}, n = 214 pairs) and RGC-SC IN pairs (r = 0.4767, p = 1.7714×10^{-6}, n = 214 pairs). However, we found pairs that show low efficacy to 1st RGC and low PSR. Taken together, we observed paired-spike enhancement in RGCs connecting

367 onto both inhibitory and excitatory SC neurons with a stronger facilitation effect for retinal afferents
368 connecting onto excitatory, in comparison to inhibitory, SC neurons.
369

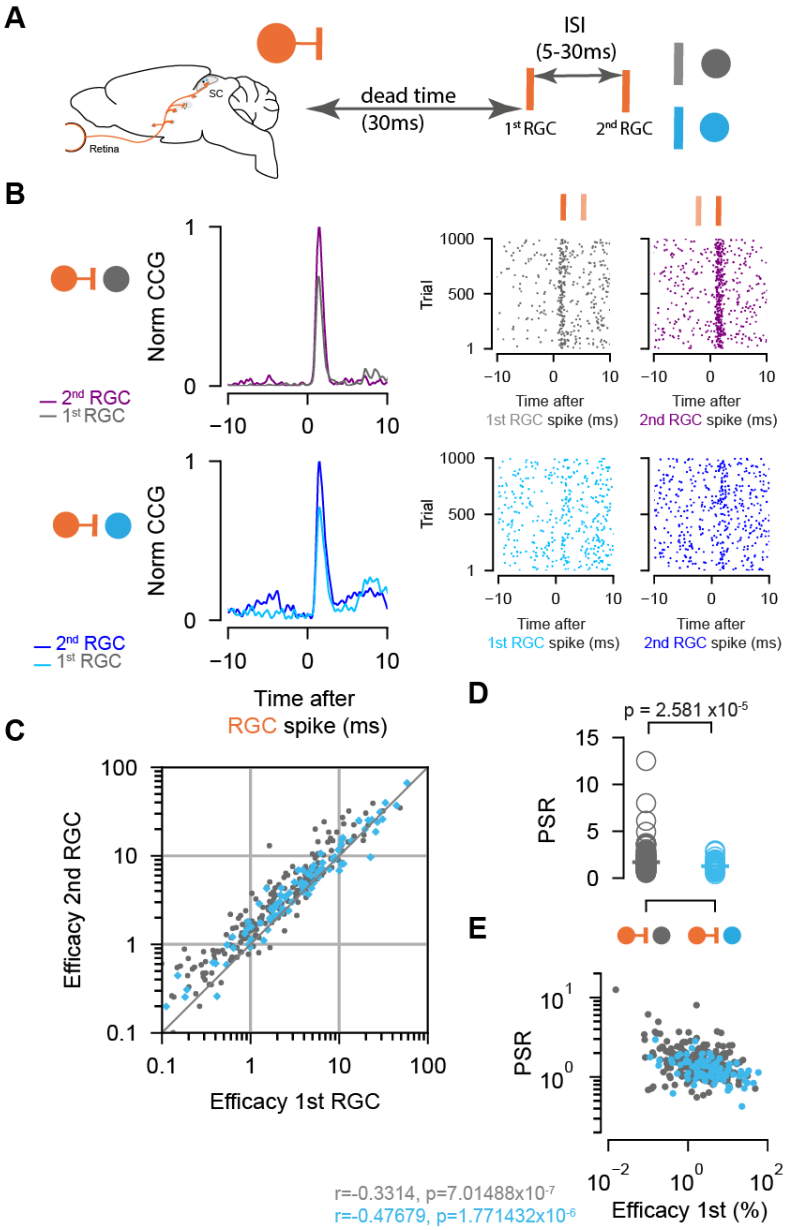

370
371
372 **Fig. 4 Paired-spike dynamics: Second retinal spikes are more efficient in driving SC response.**
373 **A,** Schematic illustrating the temporal dynamics between two successive RGC spikes. Pairs of RGC spikes
374 with a minimum inter-spike interval (ISI) of 5 ms and maximum ISI of 30 ms were included if there were no
375 preceding spikes before the 1st RGC for a dead time of at least 30ms. **B,** Cross-correlograms (CCG) of
376 example RGC-SC EXN and RGC-SC IN pairs calculated from spike trains selected for 1st and 2nd RGCs and
377 the corresponding raster plots to 1000 trials triggered on RGC spikes. **C,** Scatter plot of efficacies for 1st
378 versus 2nd retinal spikes. The majority of connected pairs (185/214 RGC-SC EXN pairs; 73/91 RGC-SC IN
379 pairs) showed paired-spike enhancement in response to 2nd RGC spikes. **D,** Paired-spike ratio (PSR) for
380 RGC-SC EXN and RGC-SC IN connected pairs. The paired pulse enhancement is stronger in SC-EXNs (n =
381 214 RGC-SC EXN; n = 91 RGC-SC IN, $p = 2.581\times10^{-5}$, two-sided Wilcoxon rank-sum test). **E,** Correlation of
382 1st RGC efficacy with the PSR for connected pairs (r = 0.3314 for n = 214 RGC-SC EXN pairs and r = 0.4767
383 for n = 91 RGC-SC IN pairs; Pearson correlation coefficient test).

384 **Inhibitory SC neurons are less coupled to the retina compared to excitatory SC neurons**

385 Our data so far reveals that excitatory and inhibitory SC neurons receive similarly strong drive from
386 their retinal afferents. However, we observed a higher mean firing rate in SC INs compared to SC
387 EXNs, on average (Fig. 1G), which is intriguing given the similarity in the RGC drive on both cell
388 types. A possible explanation could be that the activity of SC INs is less coupled to the RGC inputs
389 as compared to that of SC EXNs, i.e. SC INs spikes are less often driven by their RGC inputs. To
390 examine how strongly the activity of the two populations of SC neurons is coupled to the activity of
391 individual RGC inputs, we estimated the synaptic coupling strength from the connection contribution
392 (Levick et al., 1972; Sibille et al., 2022a; Usrey et al., 1999) of the measured retinocollicular pairs.
393 The connection contribution reflects the fraction of postsynaptic SC spikes that are preceded by a
394 presynaptic retinal spike within a short time window (Fig. 5A). High contribution values indicate that
395 SC neurons are primarily driven by individual RGC afferent inputs, while low contribution values point
396 towards an integration of multiple inputs.
397
398 Interestingly, we found that the contribution of individual retinal spikes on SC activity was higher for
399 excitatory compared to inhibitory SC neurons (Fig. 5B) (contribution RGC-SC EXN: median =
400 18.27% Q1 = 10.79%, Q3 = 29.69%, n = 214; contribution RGC-SC IN: median = 12.2%, Q1 =
401 6.61%, Q3 = 23.02%, n = 91 connected pairs, p = 0.00034694, two-sided Wilcoxon rank-sum test).
402 This opens up the possibility that SC EXNs might be more specifically linked to the retinal input
403 compared to SC INs. To assess the relationship between the coupling strength and the functional
404 similarity, we correlated both measures and found a positive correlation suggesting that stronger
405 coupled pairs show higher similarity (Fig. 5C). This correlation was higher for RGC-SC EXN pairs
406 (RGC-SC EXN r = 0.502, p = 1.0×10^{-6}, n = 85 pairs) compared to RGC-SC IN (r = 0.481, p =
407 0.0081839, n = 29 pairs, Pearson correlation coefficient test). Moreover, we observed a diversity of
408 firing rates in both SC EXNs and SC INs (Fig. 1G) which suggests that low contribution values are
409 related to the mean firing rates of the SC neurons. And indeed, when we correlated the contribution
410 to the mean firing rate, we found a negative correlation for both RGC-SC EXN and RGC-SC IN pairs
411 (RGC-SC EXN r = -0.16985, p = 0.01284; RGC-SC IN r = -0.40215, p = 0.00008, Pearson correlation
412 coefficient, n = 214 RGC-EXN; n = 91 RGC-IN connected pairs) (Fig. 5D).
413
414 Taken together, the cell-type specific difference in retinal coupling strength suggests that retinal input
415 contributes a substantial part to the spiking activity of excitatory SC neurons, while inhibitory SC
416 neurons seem to also integrate inputs from other sources. This finding denotes that excitatory SC
417 neurons are more tightly linked to the retinal input compared to inhibitory SC neurons.
418

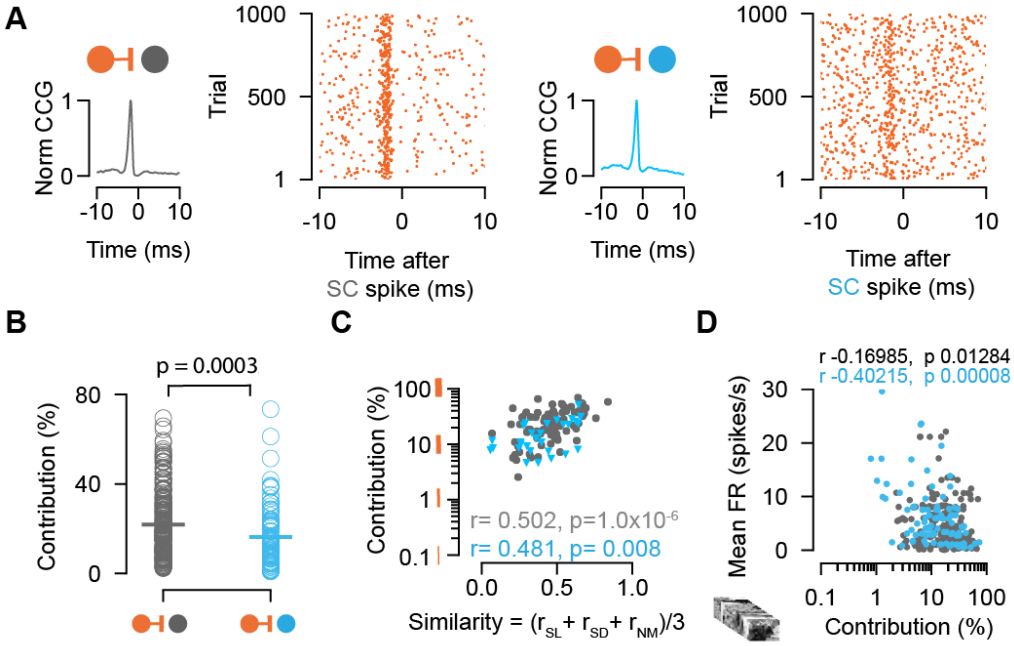

Fig. 5 Connection contribution is higher in connected RGC-SC EXN pairs. A, Example CCGs of monosynaptically connected RGC-SC EXN (top) and RGC-SC IN (bottom) pairs. Connected pairs were identified by their peaks in the CCGs (left). Raster plots of RGC spiking activity triggered on 1000 SC spikes (right). **B,** Population data on contribution measures for RGC-SC EXN and RGC-SC IN pairs (n = 114 RGC-SC EXN pairs, n=91 RGC-SC IN pairs, p = 0.0003, two-sided Wilcoxon rank-sum test). **C,** Relationship between functional similarity index and connection contribution (Pearson correlation coefficient test; n = 85 RGC-SC EXN pairs, n = 29 RGC-SC IN pairs). **D,** Correlation of mean firing rate (to natural movie stimulus) and contribution for RGC-SC EXN and RGC-SC IN pairs (Pearson correlation coefficient, two-sided Wilcoxon rank-sum test, n = 214 RGC-EXN and n = 91 RGC-IN connected pairs; n = 11 penetrations from 9 mice).

DISCUSSION

In this study, we elucidate how inhibitory and excitatory SC neurons integrate visual information from the retina *in vivo*. By combining the tangential Neuropixels recording approach with optotagging techniques, we were able to measure RGC-SC connected pairs in a cell-type specific manner and study their functional organization. Our findings allow the following conclusions: (1) The retinal drive is similarly strong for RGCs connecting onto GABAergic and non-GABAergic SC neurons. (2) The connection strength between the RGCs and both SC cell classes is positively correlated with their functional similarity, while still allowing for the presence of strong connections with low functional similarity. (3) Paired-spike enhancement in RGC-SC connections was a signature for both excitatory and inhibitory SC neurons. Finally, (4) the contribution of a retinal spike to overall SC firing is higher in excitatory SC neurons compared to inhibitory SC neurons.

We studied retinocollicular connectivity strength and aimed to answer the question whether excitatory and inhibitory SC populations use similar or different coding schemes to integrate visual information compared to the thalamocortical visual system. Connectivity patterns and circuit motifs have been extensively studied in the thalamocortical system, yet our understanding of the encoding mechanisms that govern retinocollicular signaling remains rudimentary albeit recent studies suggested that feedforward inhibition might be at play (Villalobos et al., 2018; Whyland et al., 2020). While cortical inhibitory neurons are more strongly activated by thalamic axons compared to excitatory neurons (Bruno and Simons, 2002; Cruikshank et al., 2007; Ji et al., 2016), our results now show that in the SC, the afferent retinal drive is comparably strong on excitatory and inhibitory neurons. This finding is intriguing and suggests that the two major visual brain structures in the vertebrate brain, the visual cortex and the SC, integrate afferent sensory information differentially.

Several parameters for example the degree of convergence (Kara and Reid, 2003), response properties (Alonso et al., 2001), synaptic mechanisms (Cruikshank et al., 2007) or spiking patterns (Usrey et al., 1998) can have meaningful effects on modulating the input strength on the target cell. SC neurons receive input from a small number (~6) of RGCs (Chandrasekaran et al., 2007). In contrast, cortical neurons receive numerous (approximately one order of magnitude more) thalamic inputs that are usually weak (Bruno and Sakmann, 2006; Jin et al., 2011; Lien and Scanziani, 2018). Overall, we observed strong retinal drive onto both SC populations indicated by high efficacy values (Fig. 2). One hypothesis is that convergence might be low in retinocollicular pairs as recently suggested by Sibille et al. (2022); however, despite the limited input from RGCs, these inputs may be sufficiently strong to drive the SC. This is in contrast to thalamocortical inputs, where individually efficacy values are low, but the thalamic drive is boosted by synchronously active thalamic inputs (Alonso et al., 1996; Bruno and Sakmann, 2006). Our recording method allows for the simultaneous

recording of multiple RGC afferents from SC neurons making it possible to evaluate how the synchrony among RGC afferents modulates the firing of postsynaptic SC neurons in future studies.

The difference in connection strength between cortical excitatory and inhibitory neurons could be partly attributed to their differences in response properties. Cortical inhibitory neurons display higher sensitivity, receive more convergent thalamic input, have higher firing rates and sample more randomly while excitatory neurons receive highly functional specific thalamic input (Kyriazi et al., 1994; Reid and Alonso, 1995; Simons and Carvell, 1989). While we observed higher firing rates in inhibitory SC neurons (Fig. 1G), the efficacy of the RGC-SC connections was comparable between both types of neurons (Fig. 2F), suggesting that the sensitivity of both neuron types is not markedly disparate. In general, visual response properties between excitatory and inhibitory neurons in the SC may not differ to such a great extent (Inayat et al., 2015; Kasai and Isa, 2016; Shi et al., 2017), (but see Barchini et al., 2018; Li and Meister, 2022), and experiments in the inferior colliculus show that GABAergic and glutamatergic cells share similar response properties (Ono et al., 2017). These observations imply that in the SC and other parts of the midbrain, the cell-type specific difference in terms of selectivity might not be as strongly separated as in the cortex. Future studies are required to deeper investigate the differences in response properties of the subclasses of SC neurons and whether these properties are correlated to the RGC-SC connection strength.

In our results, we observed an overall trend that functionally similar RGC-SC pairs show stronger connections which was true for both excitatory and inhibitory pairs (Fig. 3). However, we also find pairs with considerably strong retinocollicular connectivity (efficacy values >10%) albeit the functional similarity between these connected cells was low (Fig. 3D). This observation suggests that SC neurons may either show high projection-specificity by integrating inputs from a functional homogeneous population of RGCs (Li and Meister, 2022; Shi et al., 2017; Sibille et al., 2022a) or receive diverse inputs from multiple functional RGC types (Li and Meister, 2022; Sibille et al., 2022a). Moreover, a high degree of projection-specificity was recently shown to be maintained even disynaptically towards brain regions downstream of the SC (Reinhard et al., 2019), suggesting that at least one important role of the RGC-SC projection is to preserve the representation of the functionally diverse retinal channels (Baden et al., 2016). In our study, we investigated the functional similarity between connected RGC-SC pairs in response to sparse noise and natural movie stimuli. And while we observed a diversity among the similarities between RGCs and connected SC neurons, supporting the idea that SC neurons may follow diverse wiring motifs (Sibille et al., 2022a), we observed no clear difference between inhibitory and excitatory SC neurons (Fig. 3C). To further address the influence of functional properties on wiring mechanisms, it would be interesting to target the pool of different RGC types and to study how strongly they recruit SC subpopulations and modulate postsynaptic responses.

Temporal dynamics of presynaptic activity patterns are known to play a role in modulating synaptic strength (Usrey et al., 1998; Zucker, 1989). To study how the temporal spiking pattern of the RGC activity shapes RGC-SC connectivity, we analyzed the paired-spike dynamics. Across the population, we found a facilitating effect where responses to 2nd retinal spikes were more efficient in driving SC activity for both SC neuron populations. However, the paired-spike enhancement was more pronounced for excitatory than inhibitory neurons (Fig. 4). Moreover, our observation highlights differences in the encoding strategies used by different regions of visual processing. While retinogeniculate connections show paired-spike enhancement (Usrey et al., 1998), thalamocortical and corticotectal synapses express mostly depressing dynamics (Bereshpolova et al., 2006; Swadlow et al., 2002; Swadlow and Gusev, 2001), but see (Usrey et al., 2000). Our data now reveals that retinocollicular connections facilitate, suggesting that the temporal integration of RGC inputs by SC neurons may be similar to the visual thalamus.

In our study, we used cross-correlograms that were calculated from spike trains throughout the full recording period, to be applied on different connectivity strength measures. However, paired-spike dynamics are known to be modulated by the local temporal structure of inputs, for example the visual stimulus presented (Usrey et al., 1998). In addition, facilitating and depressing effects can change with the target population (Bereshpolova et al., 2006). Further studies are required to investigate whether the facilitating effect observed in our study changes upon targeting defined collicular subpopulations that may have differences in firing rates or during different stimulus conditions (e.g. spontaneous and stimulus evoked). In this study, retinocollicular connectivity was measured in anesthetized conditions. For future studies it would be interesting to examine connectivity dynamics and innervation strength in awake conditions as it has been shown that retinocollicular synapses are modulated by the animals' level of arousal (Schröder et al., 2020).

Despite our observation that retinal drive is similarly strong onto both SC cell types, the contribution of retinal activity to individual SC neurons firing was higher in excitatory SC neurons. This opens up the possibility that excitatory SC neurons may be more specifically linked to retinal inputs, while GABAergic SC cells might receive excitation from other sources aside from the retina. This finding raises the question on what other sources could drive spiking in inhibitory SC neurons?

1) RGCs provide the main input to the superficial SC (Ellis et al., 2016) with limited convergence (Sibille et al., 2022a). Nonetheless, the convergence may be higher for RGCs connecting onto inhibitory SC neurons which could explain the lower contribution and higher mean firing rates we found in inhibitory neurons. However, it has to be considered that our *in vivo* recording technique is limited in capturing the total pool of converging RGC inputs on a neuron (Sibille et al., 2022a). Viral retrograde transsynaptic tracing methods (Muellner and Roska, 2023; Rompani et al., 2017), could be employed to study the full presynaptic RGC pool of single SC neurons.

2) In addition to retinal inputs, the SC receives extensive projections from the visual cortex (V1) that could act as a potential candidate to excite inhibitory neurons. And while indeed GABAergic horizontal cells have been shown to receive V1 input (Whyland et al., 2020), the majority (93%) of corticotectal terminals target the dendrites of non-GABAergic neurons in the SC (Masterson et al., 2019). Therefore, more work is needed and studying V1 excitation to defined inhibitory subpopulations will be an important topic to be investigated by the use of tracing studies and will shed light into this complexity.

3) Intracollicular connections can provide a source of recurrent excitation on SC neurons, amplifying the retinal drive (Shi et al., 2017). However, the cell-type specificity of the intracollicular amplification is still debated. For example, while GAD2-positive horizontal cells get excitatory inputs from stellate cells (Gale and Murphy, 2018), intracollicular connectivity originating from neighboring excitatory cell types such as narrow-field (NF) and wide-field (WF) cells has shown to be rare (Gale and Murphy, 2018). Next-generation *in vitro* multi-neuron patch-clamp recordings (Campagnola et al., 2022) could reveal important new insights into the cell-type specific (Ayupe et al., 2023) intracollicular wiring.

4) In addition, collicular neurons in the visual layers also get inputs from deeper SC layers. However, excitatory connections from deep SC to the upper layers are rather uncommon (Gale and Murphy, 2018; Ghitani et al., 2014). Despite these studies have highlighted different sources of excitation onto inhibitory SC neurons, further studies are required that elucidate the role and strength of input that deep SC layers or external sources provide to drive inhibitory SC populations.

In this study, we recorded populations of well-isolated single units including RGCs as well as GABAergic and non-GABAergic SC neurons in VGAT-ChR2 mice *in vivo*. Our approach using VGAT-ChR2 mice to target all types of inhibitory SC neurons that express the vesicular GABA transporter VGAT enables a first impression on how inhibitory neurons sculpt retinocollicular signaling. Our inhibitory population is made up of 30% of the recorded SC neurons and connected pairs. These observations are in line with previous findings showing that in the upper SC layers, a substantial part of neurons (30%) are GABAergic (Ranney Mize, 1992; Whyland et al., 2020) and that around one third of the postsynaptic targets of retinocollicular terminals are GABAergic (Boka et al., 2006; Whyland et al., 2020). Yet, in spite of this high density of GABAergic neurons in the SC, they comprise of a high diversity of subpopulations that have been shown to be involved in distinct visual processing (Barchini et al., 2018; Kasai and Isa, 2016) and visually guided behaviors for example prey capture (Hoy et al., 2019) or saccadic suppression (Phongphanphanee et al., 2011). An understanding of the connectivity and encoding principles of these diverse subpopulations provides the foundation for a deeper understanding of how inhibition shapes functional circuits and their underlying behavior.

In the last decade, the diversity of SC cell types has been mainly characterized based on morphology and response properties (Franceschi and Solomon, 2018; Ito et al., 2017). Advanced techniques have started to shed light on this diversity by providing cell-type characterizations on the molecular level (Barchini et al., 2018; Gale and Murphy, 2018, 2014; Li and Meister, 2022; Villalobos et al., 2018). Three categories of potential GABAergic interneurons have been classified in the SC by the use of Cre-lines (Whyland et al., 2020) that can be further subdivided into intrinsic interneurons and potential projection neurons. RNA-sequencing has become an approach to characterize defined subtypes of neuronal populations. A recent study by Tsai et al. (2022) has mapped retinocollicular connectivity by targeting specific RGC-SC circuits using a novel approach (Trans-Seq) to classify subsets of SC cell-types that are innervated by genetically defined RGC types (Tsai et al., 2022). They identified five inhibitory clusters of retinorecipient SC cells that allow to specifically map retinocollicular connectivity. In addition, 12 distinct inhibitory subtypes have been recently identified using single-nucleus RNA sequencing where Pax7 was shown to be exclusively expressed in inhibitory neurons (Ayupe et al., 2023). Thus, we are at an enthralling stage where information on SC cell-types finally becomes available based on gene expression patterns, alike to the cortical circuit (Tremblay et al., 2016). However, while these novel techniques shed light on the diversity of inhibitory subpopulations and allow to map cell-type specific connectivity, these methods cannot provide insights into the strength of the RGC-SC connections. Hence, a key step forward would be to leverage the tracing and transcriptomics studies and combine these methods with our high-density recording approach to enable a finer characterization of the collicular interneuron diversity and the complexity of their connectivity patterns *in vivo*.

Taken together, our study targeted a heterogeneous population of GABAergic neurons in VGAT-ChR2 mice and our results reveal that excitatory and inhibitory neurons in the two main brain areas for visual processing, the visual cortex and the superior colliculus, integrate sensory afferent inputs in different ways.

ACKNOWLEDGEMENTS

We thank J. Poulet for providing us the VGAT-ChR2 mice; KL. Teh, T. Lupashina, J. Kosubek-Langer and P. Norton for comments on the manuscript. We thank the Neuropixels community for their support. This work was supported by the DFG Emmy-Noether grants KR 4062/4–1 and KR 4062/4–2 (JK).

AUTHOR CONTRIBUTIONS

C.G. and J.K. conceived and designed the study; C.G. collected the data; C.G., J.S., and J.K. analyzed the data and C.G. and J.K. wrote the manuscript with inputs from all authors.

DECLARATION OF INTERESTS

The authors declare no competing interests.

MATERIALS AND METHODS

Experimental Design

Animals

All experiments were carried out in accordance with the guidelines given by Landesamt für Gesundheit und Soziales (LAGeSo - G 0142/18) Berlin and were approved by the authority. Adult VGAT-ChR2 (Slc32a1-COP4∗H134R/EYFP, The Jackson Laboratory, stock no. 014548, n= 9) transgenic mice of either sex were used to activate inhibitory neurons (Zhao et al., 2011). Mice were aged 7-9 months old on the day of recordings.

Surgical procedures

All experiments were conducted in VGAT-ChR2 mice of both sexes. Mice were induced with 2.0-2.5% isoflurane (CP-Pharma) in an induction chamber and transferred to the surgery. Once anesthetized, the surgery was performed in a stereotactic frame (Narishige) with a closed-loop temperature controller (FHC DC) for monitoring the animal's body temperature and maintaining it at 37°C. The isoflurane level was gradually lowered during surgery and maintained at 0.8-1.5% while ensuring a complete absence of vibrissa twitching or responses to tactile stimulation. During surgery, the eyes were protected with eye ointment (Vidisic, Bausch+Lomb). Mice were head-fixed in the frame, and the skull was exposed. The head was aligned along the anterior-posterior axis and marks were made for the craniotomy at 600-1500 µm ML and 0-1500 µm AP from Lambda (Paxinos and Franklin, Nixdorf 2007 stereotactic atlas) using a micromanipulator (Luigs and Neumann). For optotagging experiments, an additional mark for the optic fiber placement was made at 3500 µm AP, 500-1200 µm ML to Bregma. A headpost was placed on the skull and implanted with dental cement (Paladur). Dental cement was also used to build a recording chamber to provide a bath for grounding. During this step, a silver wire (AG-10W, Science Products) was attached to the dental cement

652 chamber for grounding. It is important to keep the dental cement chamber low enough on the anterior
653 and posterior sides to allow for the shallow angle probe and fiber implantations, see Sibille et al
654 (2022) for a detailed description of the method (Sibille et al., 2022b). Craniotomies were made at the
655 marked positions using a dental drill (Johnson-Promident). To allow for the probe insertion at a
656 horizontal angle between 15° and 20°, a small part of the skull at the posterior part of the craniotomy
657 was slightly thinned using the drill to ensure a smooth insertion (Sibille et al., 2022b).
658

659 Anesthetized extracellular recordings and optogenetic stimulation

660 Electrophysiological recordings in SC were performed in 9 anesthetized mice of both sexes (4
661 female, 5 male) using Neuropixels 1.0 probes (Jun et al., 2017). Data were acquired at a sampling
662 rate of 30 kHz using the Open Ephys acquisition software and GUI (Siegle et al., 2017) (www.open-
663 ephys.org) and the PXIe hardware acquisition system (National Instrument NI-PXIe-1071). The
664 signal was amplified and stored in both the local field potential band (LFP, high pass-filtered 0-300
665 Hz) and the action potential band (AP, 300 Hz to 3 kHz). The tangential recordings along the anterior-
666 posterior axis in SC were performed as described in Sibille et al. (2022) (Sibille et al., 2022a). The
667 fiber for optogenetic stimulation was inserted in the SC prior to the Neuropixels probe implantation
668 to decrease mechanical pressure and reduce drift of the electrode probe. The angled optogenetic
669 fiber was zeroed at the brain surface and inserted from the anterior in a 60-70° angle towards the
670 AP axis (see Fig. 1A) and slowly lowered using a manual micromanipulator until reaching an insertion
671 of 150-200 µm. Following the fiber implantation, the Neuropixels probe was inserted tangentially in
672 a 15 to 20° angle in the superior colliculus (SC) using a micromanipulator (NewScale). The probe
673 was zeroed at Lambda and inserted 500-1200 µm ML and 2800-3800 µm DV. After the Neuropixels
674 probe was implanted, the optic fiber was lowered further slowly (to a maximum insertion depth of
675 ~250 µm) and LED pulses were applied to test for optogenetic activation of cells. After correct
676 placement, the probe and fiber were allowed to settle for 15-20 minutes before data acquisition was
677 started. In addition, confirmation of probe placement within the SC was done via receptive field (RF)
678 mapping to check the number of channels with RFs. RFs were estimated from the multi-unit activity
679 (MUA) using spike-triggered average (STA) (Sibille et al., 2022b)) (Fig. 1C).
680

681 Optotagging to identify GABAergic neurons in VGAT-ChR2 mice

682 We identified ("optotagged") populations of single GABAergic SC neurons via Channelrhodopsin-2
683 (ChR2) activation in VGAT-ChR2 mice. The optic fiber was calibrated prior to each experiment to
684 ensure a stable light output (2.5mW) measured at the fiber tip. Before the electrode probe insertion
685 (see above), the optic fiber (NA .66, 200 µm core diameter, with a bare fiber tip, PlexBright, Plexon)
686 coupled to a blue (470 nm) LED module (PlexBright, Plexon) was inserted using a 60-70° angle tilted
687 towards the AP axis (Fig. 1A). Blue light pulses were used to evoke spiking activity in VGAT-
688 expressing neurons and to verify the proper alignment of the optic fiber and the Neuropixels probe.

689 If no optogenetically evoked neuronal activity was observed, either the fiber was lowered to a
690 maximum of 250 µm or the probe position was re-adjusted to ensure both the activation and
691 recording of GABAergic SC neurons. Once the Neuropixels electrode probe and optic fiber were
692 properly aligned, optogentic stimulation using either a square wave or Gaussian function stimulus
693 pulse was applied to identify light-activated channels (Fig. 1A, B). As the stimulation using a square
694 wave pulse led to the induction of light artefacts in the spiking response (Jun et al., 2017), we
695 manually removed these artefacts in a post-processing step by interpolating the raw values in each
696 channel during the onset and offset of the square pulse in 2 out of 11 experiments. In order to
697 decrease light artefacts induced by the sharp light onset in the square wave pulse, we changed the
698 pulse to using a Gaussian function stimulus pulse to gradually increase light intensity in the
699 remaining 8 experiments. The light pulses were applied during spontaneous conditions (presentation
700 of a black background, 100 ms pulse duration, 2 Hz, 200 trials, 2.7- 3.5 mW measured at the fiber
701 tip) and conditions with visually evoked activity (checkerboard stimulus, 1000 ms pulse duration, 30
702 trials ON, 30 trials OFF, 2.7- 3.5 mW measured at the fiber tip, n = 10/11 experiments). Both
703 stimulation protocols were shown twice within the recording to ensure stable responses throughout
704 the recording session. GABAergic neurons were identified by their increased short-latency
705 responses to blue light stimulation pulses. When we compared the visually evoked responses to
706 those induced by ChR2 activation we found that they varied in their temporal activation profile (Fig.
707 1B, C). The response to the visual sparse noise stimulus starts ~80ms after the stimulus onset (Fig.
708 1C) while responses induced by ChR2 activation had a shorter latency following light onset (Fig.
709 1C).
710
711 Visual stimulation
712 Visual stimuli were generated in Python using the PsychoPy2 toolbox (Peirce et al., 2019). The visual
713 stimuli were displayed on a calibrated screen (Dell, refresh rate = 120 Hz, mean luminance = 120
714 cd/m²). For receptive field mapping, we presented the sparse noise visual stimulus on a grid of 24x
715 14 squares. The sparse noise targets were either dark (on light background) or light (on dark
716 background) and 10 deg in size with [n_targets per frame, n_trials per position] = [2,20] and
717 presented for 100 ms. A set of standardized different visual stimuli was presented including a natural
718 movie (30 trials, randomized with other stimuli, 10s) taken from Froudarakis et al. (2014)
719 (Froudarakis et al., 2014) and a full-field chirp stimulus (Baden et al., 2016). The frametimes of the
720 visual stimuli were marked by stimulus-locked synchronizing events (TTLs).
721
722 Histology
723 For histological reconstruction of the electrode track, the probe was removed, coated with
724 fluorescent dye (DiI, Abcam-ab145311) and re-inserted in the same location. In a few experiments
725 we performed multiple recordings and only stained the last insertion. Subsequently, the animal was

726 terminated with an excess of isoflurane (> 4%). Cardiac perfusion was performed with phosphate
727 buffer saline (PBS) followed by 4% paraformaldehyde (PFA) in PBS. Brains were post-fixed
728 overnight in 4% PFA, and stored in PBS until slicing (100 µm) on a vibratome (Leica VT1000S). The
729 brain slices were mounted using a mounting medium containing DAPI (DAPI-Flouromount-G, Biozol
730 Cat. 0100-20). Slices were imaged on a fluorescence microscope using a 2.5 x objective for post
731 hoc visualization of the electrode probe track.
732
733 Data analysis and statistical analyses
734 Data analysis was performed in Python 3 .0 (www.anaconda.com) using custom-written scripts.
735 MATLAB 2019b (www.mathworks.com) was used for spike sorting, see below. Statistical tests were
736 performed using the two-sided Wilcoxon rank-sum test for unpaired samples and the Wilcoxon
737 signed-rank test (two-sided) for paired samples using the scipy.stats module in Python, unless stated
738 otherwise. For correlation analyses we used Pearson correlation implemented via the linregress
739 function. Population results are indicated as mean ± standard deviation if not stated otherwise. The
740 number of neurons and animals used in each analysis is reported in the Results section or figure
741 legends.
742
743 Multi-unit activity extraction
744 For MUA analysis, common average referencing was applied to the bandpass filtered AP data
745 (Butterworth filter order 2, 0.3 to 3 kHz), where each event is extracted using custom-written Python
746 scripts. Spike detection was performed for each channel independently at a threshold of 4 standard
747 deviations in the AP band (double side detection). The scripts for performing the MUA analysis are
748 available on the GitHub repository (https://github.com/KremkowLab/tangential_recording)
749
750 Offline Spike sorting and criteria for unit classification
751 KiloSort2 and 3 (Pachitariu et al., 2016) (https://github.com/MouseLand/Kilosort) were used for
752 automatic detection and clustering of spikes followed by manual curation using phy2 (Rossant et al.,
753 2016) (https://github.com/cortex-lab/phy). Double-counted spikes were removed for each cluster
754 (within ± 0.16 ms) (Siegle et al., 2021). Furthermore, clusters with between-unit overlapping spikes
755 that show above chance zero-lag peaks in the cross-correlograms (CCG, peak windows ± 0.5 ms)
756 were re-evaluated individually in phy to be either refined or removed. Inter-spike-interval (ISI)
757 violations were calculated as the ratio of the spikes within the refractory period (± 1.5 ms) to the total
758 number of spikes. Units with ISI > 0.05% were removed. We also checked for stable firing of clusters
759 throughout the recording. Furthermore, we excluded units from further analysis that were lying
760 outside the optogenetic stimulation range (see below, Identification of Inhibitory neurons, see Fig.
761 1B) and outside the SC borders (from STA RFs on MUA, see Fig. 1C).
762

763

764 Waveform classification to identify RGC axons and SC neurons

765 A waveform classification approach was applied to distinguish action potentials (APs) from retinal
766 ganglion cell (RGC) axons and somatic APs from SC neurons (Sibille et al., 2022a). In brief, we
767 calculated the multi-channel waveform (MCW) which reflects the spatiotemporal profile of the AP
768 signals. Afferent axons and somatic signals could be classified based on their distinct waveform
769 which allowed us to classify clusters into afferent axon AP vs somatic AP. In essence, due to the SC
770 electrode probe implantation along the anterior-posterior (AP) axis, the electrode captures signals
771 from retinal axons that innervate the SC along the electrode channels. This propagation of RGC
772 axonal action potentials along the axonal path is visible in the spatiotemporal profile of their multi-
773 channel waveforms (Fig. 1D, left).

774

775 Waveform classification approach to separate GABAergic and non-GABAergic SC neurons

776 We performed standard waveform analyses to attempt to separate GABAergic SC neurons based
777 on waveform features (Jia et al., 2019; Quirk et al., 2009) (Supplementary Fig. 1). Briefly, we
778 detected the negative (trough) and positive peak (peak) from single-channel waveforms and
779 calculated their peak-to-trough duration. The amplitude was defined as the absolute difference
780 between trough and peak. The peak-to-trough ratio was defined as the ratio between amplitudes of
781 peak and trough.

782

783 Post hoc separation of GABAergic and non-GABAergic SC neurons

784 To study retinal input integration in a cell-type specific manner, we used a method to separate the
785 neural responses of GABAergic neurons from that of excitatory neurons in the SC. First, we identified
786 the minimum and maximum recording sites on the probe that were photo-activated. These borders
787 were defined via the minimum and maximum peak channel of light-induced units that are activated
788 on the probe. SC neurons that did not fall inside this optogenetic stimulation range (identified by their
789 peak channel) were excluded from further analysis. SC neurons were separated based on their
790 short-latency increase in responses to blue light pulses during two different protocols: (1) baseline
791 activity (black background, 100 ms pulse duration, 2 Hz pulse frequency) and (2) during a
792 checkerboard stimulus (1000 ms pulse duration, 30 trials LED ON, 30 trials LED OFF). This
793 classification was done using a custom-written graphical-user-interface (GUI) approach where units
794 were labeled as either “light-responsive”, “non light-responsive”. The labeling step was conducted
795 by three independent observers. A unit was included if 2 out of 3 observers chose the same label.
796 Units with unstable firing throughout the recording period were excluded from further analysis.

797

798

799

800 Identification of synaptically connected RGC-SC pairs

801 Monosynaptic connections between RGC axons and SC neurons were detected using established
802 methods (Bereshpolova et al., 2020; Clay Reid and Alonso, 1995; Denman and Contreras, 2015;
803 Usrey et al., 1998) based on statistically significant peaks at synaptic delays. Briefly, we calculated
804 a jittered (timescale jitter 5 ms) version of each spike train by randomizing all spike times within a
805 consecutive 10-15 ms window (Smith and Kohn, 2008). We then calculated the cross-correlation
806 between a pair of neurons both for the original (raw CCG) and the jittered spike train (jittered CCG).
807 Subtracting the jittered CCG from the raw CCG results in a jitter-corrected version of the CCG which
808 was used for monosynaptic pairs detection. Connected pairs were identified using cross-correlation
809 analysis and significant peaks (peak detection window from + 0.5 to 3.5 ms) had to extend over the
810 threshold (baseline + 4x standard deviation) for at least 5 consecutive time bins (0.1 ms resolution)
811 (as described previously, in Sibille et al. (2022) (Sibille et al., 2022a). The cross-correlations were
812 calculated using the Python pycorrelate package (https://github.com/tritemio/pycorrelate). Please
813 note that for CCG analysis, spike trains were correlated over the full recording duration, except for
814 periods with optogenetic stimulation. Latencies to peak response were calculated from the CCGs as
815 the maximum time within the response window.

816

817 Analysis of retinocollicular connection strength

818 Synaptic efficacy and contribution measures of connected RGC-SC pairs were estimated from
819 spiketrains during the entire recording session (except for optotagging periods which were excluded)
820 using standard approaches (Bereshpolova et al., 2020; Clay Reid and Alonso, 1995; Swadlow and
821 Gusev, 2002; Usrey et al., 1998). Briefly, efficacy was estimated from the baseline-corrected CCGs
822 by dividing the area of the CCG peak (baseline window: > -1 to < 0.4 ms, peak window: >0.4 to <3.5
823 ms) by the total number of presynaptic spikes. Thus, an efficacy measure of 1 (100%) would reflect
824 that for each presynaptic retinal spike, a postsynaptic spike could be detected. To estimate the
825 connection contribution, we counted the number of SC spikes that were preceded by a retinal
826 afferent spike, integrated over a time window between -3 to 0.5 ms, and divided this number by the
827 total number of SC spikes. A contribution of 1 (100%) indicates that all spikes of an SC neuron are
828 preceded by retinal afferent spikes.

829

830 Paired-spike dynamics analysis

831 For estimation of paired-spike dynamics, baseline-corrected CCGs were re-calculated triggered on
832 1st and 2nd RGCs using the same baseline and peak windows as mentioned above. We identified
833 pairs of retinal spikes (1st and 2nd RGC) for each RGC-SC connected pair (Usrey et al., 1998). Briefly,
834 a pair of retinal spikes was defined by a specific inter-spike interval (ISI) where the second RGC
835 spike followed the 1st RGC by a ISI of 5 to 30 ms. The second criterion for classifying a pair of retinal
836 spikes was a certain dead time where the 1st retinal spike was preceded by a minimum period of

silence (dead time: 30ms). The dead time criterion was applied to ensure a comparable level of activity immediately preceding all first spikes. The preceding window (> -1 to < 0.4 ms) was used as a baseline window. Paired-spike enhancement was calculated as the ratio of efficacy for the 2nd RGC to the efficacy for the 1st RGC.

Functional similarity analysis of retinocollicular connected pairs

To characterize the functional similarity between connected RGCs and the target neurons in the SC, we estimated the functional similarity index. To do so, we calculated the correlation coefficients from responses during the light and dark sparse noise (r_{SL} and r_{SD}) as well as during the natural movie stimulus (r_{NM}). The correlation of activity during sparse noise stimuli (r_{SL} and rS_D) was estimated from the spatiotemporal receptive fields (STRFs) which were calculated from the STA. The similarity during the natural movie stimulus (r_{NM}) was calculated from natural movie PSTHs. We limited this analysis step to neurons with high signal-to-noise ratio (SNR) in the visually evoked activity (SNR > 8 for the STRFs). The overall similarity index was then calculated from the averaged correlation coefficients: functional similarity index = $(r_{SD} + r_{SL} + r_{NM})/3$.

Data availability

The datasets that support the findings of this study are available from the corresponding author on request.

Code availability

Custom Python code is available from the corresponding author on request.

REFERENCES

Agmon A, Connors BW. 1992. Correlation between intrinsic firing patterns and thalamocortical synaptic responses of neurons in mouse barrel cortex. *J Neurosci Off J Soc Neurosci* **12**:319–329. doi:10.1523/JNEUROSCI.12-01-00319.1992

Alonso J-M, Swadlow HA. 2005. Thalamocortical specificity and the synthesis of sensory cortical receptive fields. *J Neurophysiol* **94**:26–32. doi:10.1152/jn.01281.2004

Alonso J-M, Usrey WM, Reid RC. 2001. Rules of Connectivity between Geniculate Cells and Simple Cells in Cat Primary Visual Cortex. *J Neurosci* **21**:4002–4015. doi:10.1523/JNEUROSCI.21-11-04002.2001

Alonso JM, Usrey WM, Reid RC. 1996. Precisely correlated firing in cells of the lateral geniculate nucleus. *Nature* **383**:815–819. doi:10.1038/383815a0

Ayupe AC, Choi JS, Beckedorff F, Mccartan R, Levay K, Park KK. 2023. Single-Nucleus RNA Sequencing of Developing and Mature Superior Colliculus Identifies Neuronal Diversity and Candidate Mediators of Circuit Assembly. *BioRxiv Prepr Serv Biol* 2023.02.01.526254. doi:10.1101/2023.02.01.526254

Baden T, Berens P, Franke K, Román Rosón M, Bethge M, Euler T. 2016. The functional diversity of retinal ganglion cells in the mouse. *Nature* **529**:345–350. doi:10.1038/nature16468

Barchini J, Shi X, Chen H, Cang J. 2018. Bidirectional encoding of motion contrast in the mouse superior colliculus. *eLife* **7**:e35261. doi:10.7554/eLife.35261

Bereshpolova Y, Hei X, Alonso J-M, Swadlow HA. 2020. Three rules govern thalamocortical connectivity of fast-spike inhibitory interneurons in the visual cortex. *eLife* **9**:e60102. doi:10.7554/eLife.60102

Bereshpolova Y, Stoelzel CR, Gusev AG, Bezdudnaya T, Swadlow HA. 2006. The impact of a corticotectal impulse on the awake superior colliculus. *J Neurosci Off J Soc Neurosci* **26**:2250–2259. doi:10.1523/JNEUROSCI.4402-05.2006

Boka K, Chomsung R, Li J, Bickford ME. 2006. Comparison of the ultrastructure of cortical and retinal terminals in the rat superior colliculus. *Anat Rec A Discov Mol Cell Evol Biol* **288A**:850–858. doi:10.1002/ar.a.20359

Bruno RM, Sakmann B. 2006. Cortex is driven by weak but synchronously active thalamocortical synapses. *Science* **312**:1622–1627. doi:10.1126/science.1124593

Bruno RM, Simons DJ. 2002. Feedforward Mechanisms of Excitatory and Inhibitory Cortical Receptive Fields. *J Neurosci* **22**:10966–10975. doi:10.1523/JNEUROSCI.22-24-10966.2002

Campagnola L, Seeman SC, Chartrand T, Kim L, Hoggarth A, Gamlin C, Ito S, Trinh J, Davoudian P, Radaelli C, Kim M-H, Hage T, Braun T, Alfiler L, Andrade J, Bohn P, Dalley R, Henry A, Kebede S, Alice M, Sandman D, Williams G, Larsen R, Teeter C, Daigle TL, Berry K, Dotson N, Enstrom R, Gorham M, Hupp M, Dingman Lee S, Ngo K, Nicovich PR, Potekhina L, Ransford S, Gary A, Goldy J, McMillen D, Pham T, Tieu M, Siverts L, Walker M, Farrell C, Schroedter M, Slaughterbeck C, Cobb C, Ellenbogen R, Gwinn RP, Keene CD, Ko AL, Ojemann JG, Silbergeld DL, Carey D, Casper T, Crichton K, Clark M, Dee N, Ellingwood L, Gloe J, Kroll M, Sulc J, Tung H, Wadhwani K, Brouner K, Egdorf T, Maxwell M, McGraw M, Pom CA, Ruiz A, Bomben J, Feng D, Hejazinia N, Shi S, Szafer A, Wakeman W, Phillips J, Bernard A, Esposito L, D'Orazi FD, Sunkin S, Smith K, Tasic B, Arkhipov A, Sorensen S, Lein E, Koch C, Murphy G, Zeng H, Jarsky T. 2022. Local connectivity and synaptic dynamics in mouse and human neocortex. *Science* **375**:eabj5861. doi:10.1126/science.abj5861

Chandrasekaran AR, Shah RD, Crair MC. 2007. Developmental Homeostasis of Mouse Retinocollicular Synapses. *J Neurosci* **27**:1746–1755. doi:10.1523/JNEUROSCI.4383-06.2007

Clay Reid R, Alonso J-M. 1995. Specificity of monosynaptic connections from thalamus to visual cortex. *Nature* **378**:281–284. doi:10.1038/378281a0

Cruikshank SJ, Lewis TJ, Connors BW. 2007. Synaptic basis for intense thalamocortical activation of feedforward inhibitory cells in neocortex. *Nat Neurosci* **10**:462–468. doi:10.1038/nn1861

Denman DJ, Contreras D. 2015. Complex Effects on In Vivo Visual Responses by Specific Projections from Mouse Cortical Layer 6 to Dorsal Lateral Geniculate Nucleus. *J Neurosci* **35**:9265–9280. doi:10.1523/JNEUROSCI.0027-15.2015

Ellis EM, Gauvain G, Sivyer B, Murphy GJ. 2016. Shared and distinct retinal input to the mouse superior colliculus and dorsal lateral geniculate nucleus. *J Neurophysiol* **116**:602–610. doi:10.1152/jn.00227.2016

Essig J, Hunt JB, Felsen G. 2021. Inhibitory neurons in the superior colliculus mediate selection of spatially-directed movements. *Commun Biol* **4**:719. doi:10.1038/s42003-021-02248-1

Evans DA, Stempel AV, Vale R, Ruehle S, Lefler Y, Branco T. 2018. A synaptic threshold mechanism for computing escape decisions. *Nature* **558**:590–594. doi:10.1038/s41586-018-0244-6

Ferrarese L, Jouhanneau J-S, Remme MWH, Kremkow J, Katona G, Rózsa B, Schreiber S, Poulet JFA. 2018. Dendrite-Specific Amplification of Weak Synaptic Input during Network Activity In Vivo. *Cell Rep* **24**:3455-3465.e5. doi:10.1016/j.celrep.2018.08.088

Franceschi G, Solomon SG. 2018. Visual response properties of neurons in the superficial layers of the superior colliculus of awake mouse. *J Physiol* **596**:6307–6332. doi:10.1113/JP276964

Froudarakis E, Berens P, Ecker AS, Cotton RJ, Sinz FH, Yatsenko D, Saggau P, Bethge M, Tolias AS. 2014. Population code in mouse V1 facilitates readout of natural scenes through increased sparseness. *Nat Neurosci* **17**:851–857. doi:10.1038/nn.3707

Gabernet L, Jadhav SP, Feldman DE, Carandini M, Scanziani M. 2005. Somatosensory integration controlled by dynamic thalamocortical feed-forward inhibition. *Neuron* **48**:315–327. doi:10.1016/j.neuron.2005.09.022

Gale SD, Murphy GJ. 2018. Distinct cell types in the superficial superior colliculus project to the dorsal lateral geniculate and lateral posterior thalamic nuclei. *J Neurophysiol* **120**:1286–1292. doi:10.1152/jn.00248.2018

Gale SD, Murphy GJ. 2016. Active Dendritic Properties and Local Inhibitory Input Enable Selectivity for Object Motion in Mouse Superior Colliculus Neurons. *J Neurosci* **36**:9111–9123. doi:10.1523/JNEUROSCI.0645-16.2016

Gale SD, Murphy GJ. 2014. Distinct representation and distribution of visual information by specific cell types in mouse superficial superior colliculus. *J Neurosci Off J Soc Neurosci* **34**:13458–13471. doi:10.1523/JNEUROSCI.2768-14.2014

Ghitani N, Bayguinov PO, Vokoun CR, McMahon S, Jackson MB, Basso MA. 2014. Excitatory Synaptic Feedback from the Motor Layer to the Sensory Layers of the Superior Colliculus. *J Neurosci* **34**:6822–6833. doi:10.1523/JNEUROSCI.3137-13.2014

Gibson JR, Beierlein M, Connors BW. 1999. Two networks of electrically coupled inhibitory neurons in neocortex. *Nature* **402**:75–79. doi:10.1038/47035

Glickfeld LL, Histed MH, Maunsell JHR. 2013. Mouse Primary Visual Cortex Is Used to Detect Both Orientation and Contrast Changes. *J Neurosci* **33**:19416–19422. doi:10.1523/JNEUROSCI.3560-13.2013

Hoy JL, Bishop HI, Niell CM. 2019. Defined Cell Types in Superior Colliculus Make Distinct Contributions to Prey Capture Behavior in the Mouse. *Curr Biol* **29**:4130-4138.e5. doi:10.1016/j.cub.2019.10.017

Inayat S, Barchini J, Chen H, Feng L, Liu X, Cang J. 2015. Neurons in the Most Superficial Lamina of the Mouse Superior Colliculus Are Highly Selective for Stimulus Direction. *J Neurosci* **35**:7992–8003. doi:10.1523/JNEUROSCI.0173-15.2015

Inoue T, Imoto K. 2006. Feedforward inhibitory connections from multiple thalamic cells to multiple regular-spiking cells in layer 4 of the somatosensory cortex. *J Neurophysiol* **96**:1746–1754. doi:10.1152/jn.00301.2006

Isaacson JS, Scanziani M. 2011. How Inhibition Shapes Cortical Activity. *Neuron* **72**:231–243. doi:10.1016/j.neuron.2011.09.027

Ito S, Feldheim DA, Litke AM. 2017. Segregation of Visual Response Properties in the Mouse Superior Colliculus and Their Modulation during Locomotion. *J Neurosci* **37**:8428–8443. doi:10.1523/JNEUROSCI.3689-16.2017

Ji X, Zingg B, Mesik L, Xiao Z, Zhang LI, Tao HW. 2016. Thalamocortical Innervation Pattern in Mouse Auditory and Visual Cortex: Laminar and Cell-Type Specificity. *Cereb Cortex* **26**:2612–2625. doi:10.1093/cercor/bhv099

Jia X, Siegle JH, Bennett C, Gale SD, Denman DJ, Koch C, Olsen SR. 2019. High-density extracellular probes reveal dendritic backpropagation and facilitate neuron classification. *J Neurophysiol* **121**:1831–1847. doi:10.1152/jn.00680.2018

Jin J, Wang Y, Swadlow HA, Alonso JM. 2011. Population receptive fields of ON and OFF thalamic inputs to an orientation column in visual cortex. *Nat Neurosci* **14**:232–238. doi:10.1038/nn.2729

Jun JJ, Steinmetz NA, Siegle JH, Denman DJ, Bauza M, Barbarits B, Lee AK, Anastassiou CA, Andrei A, Aydın Ç, Barbic M, Blanche TJ, Bonin V, Couto J, Dutta B, Gratiy SL, Gutnisky DA, Häusser M, Karsh B, Ledochowitsch P, Lopez CM, Mitelut C, Musa S, Okun M, Pachitariu M, Putzeys J, Rich PD, Rossant C, Sun W, Svoboda K, Carandini M, Harris KD, Koch C, O'Keefe J, Harris TD. 2017. Fully integrated silicon probes for high-density recording of neural activity. *Nature* **551**:232–236. doi:10.1038/nature24636

Kaneda K, Isa K, Yanagawa Y, Isa T. 2008. Nigral Inhibition of GABAergic Neurons in Mouse Superior Colliculus. *J Neurosci* **28**:11071–11078. doi:10.1523/JNEUROSCI.3263-08.2008

Kara P, Reid RC. 2003. Efficacy of Retinal Spikes in Driving Cortical Responses. *J Neurosci* **23**:8547–8557. doi:10.1523/JNEUROSCI.23-24-08547.2003

Kasai M, Isa T. 2016. Imaging population dynamics of surround suppression in the superior colliculus. *Eur J Neurosci* **44**:2543–2556. doi:10.1111/ejn.13371

Kremkow J, Aertsen A, Kumar A. 2010a. Gating of Signal Propagation in Spiking Neural Networks by Balanced and Correlated Excitation and Inhibition. *J Neurosci* **30**:15760–15768. doi:10.1523/JNEUROSCI.3874-10.2010

Kremkow J, Alonso J-M. 2018. Thalamocortical Circuits and Functional Architecture. *Annu Rev Vis Sci* **4**:263–285. doi:10.1146/annurev-vision-091517-034122

Kremkow J, Perrinet LU, Masson GS, Aertsen A. 2010b. Functional consequences of correlated excitatory and inhibitory conductances in cortical networks. *J Comput Neurosci* **28**:579–594. doi:10.1007/s10827-010-0240-9

Kremkow J, Perrinet LU, Monier C, Alonso J-M, Aertsen A, Frégnac Y, Masson GS. 2016. Push-Pull Receptive Field Organization and Synaptic Depression: Mechanisms for Reliably Encoding Naturalistic Stimuli in V1. *Front Neural Circuits* **10**.

Kyriazi HT, Carvell GE, Simons DJ. 1994. OFF response transformations in the whisker/barrel system. *J Neurophysiol* **72**:392–401. doi:10.1152/jn.1994.72.1.392

Lashley KS. 1931. The mechanism of vision IV. The cerebral areas necessary for pattern vision in the rat. *J Comp Neurol* **53**:419–478. doi:10.1002/cne.900530304

Lee CM, Osman AF, Volgushev M, Escabí MA, Read HL. 2016. Neural spike-timing patterns vary with sound shape and periodicity in three auditory cortical fields. *J Neurophysiol* **115**:1886–1904. doi:10.1152/jn.00784.2015

Lee S-H, Kwan AC, Zhang S, Phoumthipphavong V, Flannery JG, Masmanidis SC, Taniguchi H, Huang ZJ, Zhang F, Boyden ES, Deisseroth K, Dan Y. 2012. Activation of specific interneurons improves V1 feature selectivity and visual perception. *Nature* **488**:379–383. doi:10.1038/nature11312

Levick WR, Cleland BG, Dubin MW. 1972. Lateral geniculate neurons of cat: retinal inputs and physiology. *Invest Ophthalmol* **11**:302–311.

Li Y, Meister M. 2022. Functional Cell Types in the Mouse Superior Colliculus (preprint). Neuroscience. doi:10.1101/2022.04.01.486789

Lien AD, Scanziani M. 2018. Cortical direction selectivity emerges at convergence of thalamic synapses. *Nature* **558**:80–86. doi:10.1038/s41586-018-0148-5

Masterson SP, Zhou N, Akers BK, Dang W, Bickford ME. 2019. Ultrastructural and optogenetic dissection of V1 corticotectal terminal synaptic properties. *J Comp Neurol* **527**:833–842. doi:10.1002/cne.24538

Mastronarde DN. 1987. Two classes of single-input X-cells in cat lateral geniculate nucleus. II. Retinal inputs and the generation of receptive-field properties. *J Neurophysiol* **57**:381–413. doi:10.1152/jn.1987.57.2.381

Miller KD. 2016. Canonical computations of cerebral cortex. *Curr Opin Neurobiol* **37**:75–84. doi:10.1016/j.conb.2016.01.008

Moore AK, Wehr M. 2013. Parvalbumin-expressing inhibitory interneurons in auditory cortex are well-tuned for frequency. *J Neurosci Off J Soc Neurosci* **33**:13713–13723. doi:10.1523/JNEUROSCI.0663-13.2013

Muellner FE, Roska B. 2023. Individual thalamic inhibitory interneurons are functionally specialized towards distinct visual features (preprint). Neuroscience. doi:10.1101/2023.03.22.533751

Niell CM, Scanziani M. 2021. How Cortical Circuits Implement Cortical Computations: Mouse Visual Cortex as a Model. *Annu Rev Neurosci* **44**:517–546. doi:10.1146/annurev-neuro-102320-085825

Niell CM, Stryker MP. 2008. Highly Selective Receptive Fields in Mouse Visual Cortex. *J Neurosci* **28**:7520–7536. doi:10.1523/JNEUROSCI.0623-08.2008

Ono M, Bishop DC, Oliver DL. 2017. Identified GABAergic and Glutamatergic Neurons in the Mouse Inferior Colliculus Share Similar Response Properties. *J Neurosci* **37**:8952–8964. doi:10.1523/JNEUROSCI.0745-17.2017

Pachitariu M, Steinmetz N, Kadir S, Carandini M, Kenneth D. H. 2016. Kilosort: realtime spike-sorting for extracellular electrophysiology with hundreds of channels (preprint). Neuroscience. doi:10.1101/061481

Peirce J, Gray JR, Simpson S, MacAskill M, Höchenberger R, Sogo H, Kastman E, Lindeløv JK. 2019. PsychoPy2: Experiments in behavior made easy. *Behav Res Methods* **51**:195–203. doi:10.3758/s13428-018-01193-y

Petruno SK, Clark RE, Reinagel P. 2013. Evidence that primary visual cortex is required for image, orientation, and motion discrimination by rats. *PloS One* **8**:e56543. doi:10.1371/journal.pone.0056543

Phongphanphanee P, Mizuno F, Lee PH, Yanagawa Y, Isa T, Hall WC. 2011. A Circuit Model for Saccadic Suppression in the Superior Colliculus. *J Neurosci* **31**:1949–1954. doi:10.1523/JNEUROSCI.2305-10.2011

Porter JT, Johnson CK, Agmon A. 2001. Diverse Types of Interneurons Generate Thalamus-Evoked Feedforward Inhibition in the Mouse Barrel Cortex. *J Neurosci* **21**:2699–2710. doi:10.1523/JNEUROSCI.21-08-02699.2001

Quirk MC, Sosulski DL, Feierstein CE, Uchida N, Mainen ZF. 2009. A Defined Network of Fast-Spiking Interneurons in Orbitofrontal Cortex: Responses to Behavioral Contingencies and Ketamine Administration. *Front Syst Neurosci* **3**:13. doi:10.3389/neuro.06.013.2009

Ranney Mize R. 1992. Chapter 11 The organization of GABAergic neurons in the mammalian superior colliculusProgress in Brain Research. Elsevier. pp. 219–248. doi:10.1016/S0079-6123(08)63616-X

Reid RC, Alonso JM. 1995. Specificity of monosynaptic connections from thalamus to visual cortex. *Nature* **378**:281–284. doi:10.1038/378281a0

Reinhard K, Li C, Do Q, Burke EG, Heynderickx S, Farrow K. 2019. A projection specific logic to sampling visual inputs in mouse superior colliculus. *eLife* **8**:e50697. doi:10.7554/eLife.50697

Rompani SB, Müllner FE, Wanner A, Zhang C, Roth CN, Yonehara K, Roska B. 2017. Different Modes of Visual Integration in the Lateral Geniculate Nucleus Revealed by Single-Cell-Initiated Transsynaptic Tracing. *Neuron* **93**:767-776.e6. doi:10.1016/j.neuron.2017.01.028

Rossant C, Kadir SN, Goodman DFM, Schulman J, Hunter MLD, Saleem AB, Grosmark A, Belluscio M, Denfield GH, Ecker AS, Tolias AS, Solomon S, Buzsaki G, Carandini M, Harris KD. 2016. Spike sorting for large, dense electrode arrays. *Nat Neurosci* **19**:634–641. doi:10.1038/nn.4268

Schröder S, Steinmetz NA, Krumin M, Pachitariu M, Rizzi M, Lagnado L, Harris KD, Carandini M. 2020. Arousal Modulates Retinal Output. *Neuron* **107**:487-495.e9. doi:10.1016/j.neuron.2020.04.026

Shang C, Liu A, Li D, Xie Z, Chen Z, Huang M, Li Y, Wang Y, Shen WL, Cao P. 2019. A subcortical excitatory circuit for sensory-triggered predatory hunting in mice. *Nat Neurosci* **22**:909–920. doi:10.1038/s41593-019-0405-4

Shang C, Liu Z, Chen Z, Shi Y, Wang Q, Liu S, Li D, Cao P. 2015. BRAIN CIRCUITS. A parvalbumin-positive excitatory visual pathway to trigger fear responses in mice. *Science* **348**:1472–1477. doi:10.1126/science.aaa8694

Shi X, Barchini J, Ledesma HA, Koren D, Jin Y, Liu X, Wei W, Cang J. 2017. Retinal origin of direction selectivity in the superior colliculus. *Nat Neurosci* **20**:550–558. doi:10.1038/nn.4498

Sibille J, Gehr C, Benichov JI, Balasubramanian H, Teh KL, Lupashina T, Vallentin D, Kremkow J. 2022a. High-density electrode recordings reveal strong and specific connections between retinal ganglion cells and midbrain neurons. *Nat Commun* **13**:5218. doi:10.1038/s41467-022-32775-2

Sibille J, Gehr C, Teh KL, Kremkow J. 2022b. Tangential high-density electrode insertions allow to simultaneously measure neuronal activity across an extended region of the visual field in mouse superior colliculus. *J Neurosci Methods* **376**:109622. doi:10.1016/j.jneumeth.2022.109622

Siegle JH, Jia X, Durand S, Gale S, Bennett C, Graddis N, Heller G, Ramirez TK, Choi H, Luviano JA, Groblewski PA, Ahmed R, Arkhipov A, Bernard A, Billeh YN, Brown D, Buice MA, Cain N, Caldejon S, Casal L, Cho A, Chvilicek M, Cox TC, Dai K, Denman DJ, de Vries SEJ, Dietzman R, Esposito L, Farrell C, Feng D, Galbraith J, Garrett M, Gelfand EC, Hancock N, Harris JA, Howard R, Hu B, Hytnen R, Iyer R, Jessett E, Johnson K, Kato I, Kiggins J, Lambert S, Lecoq J, Ledochowitsch P, Lee JH, Leon A, Li Y, Liang E, Long F, Mace K, Melchior J, Millman D, Mollenkopf T, Nayan C, Ng L, Ngo K, Nguyen T, Nicovich PR, North K, Ocker GK, Ollerenshaw D, Oliver M, Pachitariu M, Perkins J, Reding M, Reid D, Robertson M, Ronellenfitch K, Seid S, Slaughterbeck C, Stoecklin M, Sullivan D, Sutton B,

Swapp J, Thompson C, Turner K, Wakeman W, Whitesell JD, Williams D, Williford A, Young R, Zeng H, Naylor S, Phillips JW, Reid RC, Mihalas S, Olsen SR, Koch C. 2021. Survey of spiking in the mouse visual system reveals functional hierarchy. *Nature*. doi:10.1038/s41586-020-03171-x

Siegle JH, López AC, Patel YA, Abramov K, Ohayon S, Voigts J. 2017. Open Ephys: an open-source, plugin-based platform for multichannel electrophysiology. *J Neural Eng* **14**:045003. doi:10.1088/1741-2552/aa5eea

Simons DJ, Carvell GE. 1989. Thalamocortical response transformation in the rat vibrissa/barrel system. *J Neurophysiol* **61**:311–330. doi:10.1152/jn.1989.61.2.311

Smith MA, Kohn A. 2008. Spatial and Temporal Scales of Neuronal Correlation in Primary Visual Cortex. *J Neurosci* **28**:12591–12603. doi:10.1523/JNEUROSCI.2929-08.2008

Sun Q-Q, Huguenard JR, Prince DA. 2006. Barrel cortex microcircuits: thalamocortical feedforward inhibition in spiny stellate cells is mediated by a small number of fast-spiking interneurons. *J Neurosci Off J Soc Neurosci* **26**:1219–1230. doi:10.1523/JNEUROSCI.4727-04.2006

Swadlow HA. 2003. Fast-spike Interneurons and Feedforward Inhibition in Awake Sensory Neocortex. *Cereb Cortex* **13**:25–32. doi:10.1093/cercor/13.1.25

Swadlow HA, Gusev AG. 2002. Receptive-field construction in cortical inhibitory interneurons. *Nat Neurosci* **5**:403–404. doi:10.1038/nn847

Swadlow HA, Gusev AG. 2001. The impact of “bursting” thalamic impulses at a neocortical synapse. *Nat Neurosci* **4**:402–408. doi:10.1038/86054

Swadlow HA, Gusev AG, Bezdudnaya T. 2002. Activation of a Cortical Column by a Thalamocortical Impulse. *J Neurosci* **22**:7766–7773. doi:10.1523/JNEUROSCI.22-17-07766.2002

Tremblay R, Lee S, Rudy B. 2016. GABAergic interneurons in the neocortex: From cellular properties to circuits. *Neuron* **91**:260–292. doi:10.1016/j.neuron.2016.06.033

Tsai NY, Wang Fei, Toma K, Yin C, Takatoh J, Pai EL, Wu K, Matcham AC, Yin L, Dang EJ, Marciano DK, Rubenstein JL, Wang Fan, Ullian EM, Duan X. 2022. Trans-Seq maps a selective mammalian retinotectal synapse instructed by Nephronectin. *Nat Neurosci* **25**:659–674. doi:10.1038/s41593-022-01068-8

Usrey WM, Alonso J-M, Reid RC. 2000. Synaptic Interactions between Thalamic Inputs to Simple Cells in Cat Visual Cortex. *J Neurosci* **20**:5461–5467. doi:10.1523/JNEUROSCI.20-14-05461.2000

Usrey WM, Reppas JB, Reid RC. 1999. Specificity and Strength of Retinogeniculate Connections. *J Neurophysiol* **82**:3527–3540. doi:10.1152/jn.1999.82.6.3527

Usrey WM, Reppas JB, Reid RC. 1998. Paired-spike interactions and synaptic efficacy of retinal inputs to the thalamus. *Nature* **395**:384–387. doi:10.1038/26487

Villalobos CA, Wu Q, Lee PH, May PJ, Basso MA. 2018. Parvalbumin and GABA Microcircuits in the Mouse Superior Colliculus. *Front Neural Circuits* **12**:35. doi:10.3389/fncir.2018.00035

Wei P, Liu N, Zhang Z, Liu X, Tang Y, He X, Wu B, Zhou Z, Liu Y, Li J, Zhang Y, Zhou X, Xu L, Chen L, Bi G, Hu X, Xu F, Wang L. 2015. Processing of visually evoked innate fear by a non-canonical thalamic pathway. *Nat Commun* **6**:6756. doi:10.1038/ncomms7756

Whyland KL, Slusarczyk AS, Bickford ME. 2020. GABAergic cell types in the superficial layers of the mouse superior colliculus. *J Comp Neurol* **528**:308–320. doi:10.1002/cne.24754

Zhang Z, Liu W-Y, Diao Y-P, Xu W, Zhong Y-H, Zhang J-Y, Lazarus M, Liu Y-Y, Qu W-M, Huang Z-L. 2019. Superior Colliculus GABAergic Neurons Are Essential for Acute Dark Induction of Wakefulness in Mice. *Curr Biol CB* **29**:637-644.e3. doi:10.1016/j.cub.2018.12.031

Zhao S, Ting JT, Atallah HE, Qiu L, Tan J, Gloss B, Augustine GJ, Deisseroth K, Luo M, Graybiel AM, Feng G. 2011. Cell type–specific channelrhodopsin-2 transgenic mice for optogenetic dissection of neural circuitry function. *Nat Methods* **8**:745–752. doi:10.1038/nmeth.1668

Zucker RS. 1989. Short-term synaptic plasticity. *Annu Rev Neurosci* **12**:13–31. doi:10.1146/annurev.ne.12.030189.000305